Journal of Marine Systems 249 (2025) 104067

Contents lists available at ScienceDirect

Journal of Marine Systems

journal homepage: www.elsevier.com/locate/jmarsys

# Will the declining sea ice extent in the Arctic cause a reversal of net benthic-pelagic exchange directions?

Saskia Rühl [a,*], Charlotte E.L. Thompson [b], Ana M. Queirós [a], Joanne E. Hopkins [c], Sian F. Henley [d], Stephen Widdicombe [a]

[a] Plymouth Marine Laboratory, Prospect Place, Plymouth, Devon PL1 3DH, UK
[b] School of Ocean and Earth Science, University of Southampton, National Oceanography Centre, Southampton, European Way, Empress Dock, SO14 3ZH, UK
[c] Marine Physics and Ocean Climate, National Oceanography Centre, Joseph Proudman Building, 6 Brownlow Street, Liverpool L3 5DA, UK
[d] School of GeoSciences, University of Edinburgh, James Hutton Road, Edinburgh EH9 3FE, UK

ARTICLE INFO

*Keywords:*
Arctic Ocean
Benthic-pelagic exchange
Biogeochemical cycling
Climate change
Particles
Sea ice
Solutes

ABSTRACT

In the Arctic, loss of sea ice due to climate change and the northward shift of the Polar Front are predicted to affect many ecosystem processes such as the ecologically important process of particulate and dissolved matter exchange between the seafloor and the water column. In this study, we show for the first time that a change from an ice-covered, Arctic water-dominated system to an Atlantic -dominated ice-free one is likely to reverse seafloor-water exchange directions. A north – south transect across the Barents Sea was studied over two years with differing sea ice cover conditions, recording biological, biogeochemical, hydrographic, geophysical, and oceanographic data. There was a clear difference between the direction and magnitude of key benthic-pelagic fluxes present at Atlantic-dominated environments, and those in Arctic water – dominated ones. Currently, the southern Barents Sea exhibits a net downward flux of dissolved matter and a net upward flux of particulates, while in the northern region solutes fluctuate upwards and particulates downward, making the North a more depositional region that promotes near-surface primary productivity. Broad scale assessments of net fluxes in rapidly changing ecosystems should be employed to monitor impacts of climate change and anthropogenic activities.

## 1. Introduction

The most pressing environmental challenge of our time is global climate change, which has well documented and wide-reaching impacts on marine ecosystems around the globe (IPCC, 2019). One location where the effects of climate change can already be observed is the Arctic, one of the most rapidly changing environments on the planet due to both atmospheric and oceanic warming (Serreze and Barry, 2011). Regions such as the Barents Sea are experiencing pronounced losses of sea ice (Onarheim et al., 2018; Onarheim and Årthun, 2017), particularly due to increased advection of warm Atlantic water onto the shelf (Årthund et al., 2020; Oziel et al., 2020) and its northern region is transitioning from a cold and strongly stratified Arctic environment to a warm, more weakly stratified Atlantic-dominated climate regime (Lind et al., 2018).

The southern expression of the Polar Front (associated with strong temperature gradients) and the southern limit of seasonal sea ice have both shifted northwards over time, in response to local warming and increased advection of warmer water (Barton et al., 2018; Ingvaldsen, 2005; Oziel et al., 2016), by roughly 150 km since the 1960 (Ivshin et al., 2019). There are large inter-annual variations in the extent of the sea ice due to climate cycles such as the Arctic Oscillation (Fyfe et al., 1999; Wang and Ikeda, 2000; Rigor et al., 2002; Barton et al., 2018) and variations in heat influx from Atlantic waters (Årthund et al., 2020). A decline in sea ice is very likely to affect both pelagic and benthic environments, as the two have been shown to be tightly coupled (see Rühl et al., 2020b; Grebmeier and Barry, 1991; Ambrose and Renaud, 1995; Olli et al., 2002; Renaud et al., 2007). Productivity of benthic fauna in Arctic shelf regions is highly dependent on energy and matter input through downward flux of organic matter (OM) from pelagic phytoplankton blooms (Wassmann et al., 1996; Aschan and Trannum, 2006; Tamelander et al., 2006; Renaud et al., 2008; Cochrane et al., 2009) and seasonal ice algae sinking (Riebesell et al., 1991; McMahon et al., 2013).

* Corresponding author.
*E-mail addresses:* sru@pml.ac.uk (S. Rühl), celt1@noc.soton.ac.uk (C.E.L. Thompson), anqu@pml.ac.uk (A.M. Queirós), jeh200@noc.ac.uk (J.E. Hopkins), s.f.henley@ed.ac.uk (S.F. Henley), swi@pml.ac.uk (S. Widdicombe).

https://doi.org/10.1016/j.jmarsys.2025.104067
Received 22 March 2024; Received in revised form 21 March 2025; Accepted 12 April 2025
Available online 29 April 2025

The nature and magnitude of potential vertical OM export through the water column are shaped by water column stratification and zooplankton activity (Olli et al., 2002). Although warmer years have been linked to higher rates of productivity (Sakshaug, 1997), a loss of sea ice is likely to affect the quantity, quality and timing of OM input to the benthos (see e.g. Wassmann et al., 1996). Increased OM input could lead to a change in benthic macrofauna biomass in the northern regions (Cochrane et al., 2009). Furthermore, benthic areas which had previously been protected by the ice cover in winter may become accessible and be disturbed year-round through anthropogenic actions such as trawling (Misund et al., 2016).

Each of these climate-driven changes (to OM production and vertical export, benthic faunal activity and community composition, frequency of anthropogenic disturbance, etc.) has the potential to cause shifts in fundamental processes at the ecosystem level. One such process is the movement of dissolved and particulate matter (hereafter, DM and PM) throughout the marine environment. Vertical exchanges of DM and PM between the sediment and overlying water (as characterized in Rühl et al., 2020b) are a vital component of many biologically important ecosystem processes, such as OM, carbon and nutrient cycling (Giraud et al., 2008; Griffiths et al., 2017). Direct drivers of DM exchange are diffusion, advection, physical resuspension, biological particle mixing and bioirrigation (Rühl et al., 2020b). PM exchange, on the other hand, is best characterized through the main directions in which it can take place: deposition / downward transport and resuspension / upward transport (Rühl et al., 2020b).

A shift between the various sources and sinks of OM in an area could lead to changes in the nature and intensity of local benthic-pelagic (B—P) exchange pathways (Rühl et al., 2020a, 2020b). Changes to the benthic macrofauna community through lowered OM quantity and quality, new non-indigenous species, and/or trawling may perpetuate changes in biologically driven DM and PM flux pathways such as bioturbation and bioirrigation (see e.g. Maiti et al., 2010). The northward movement of the Polar Front and seasonal ice edge, may lead to lower biological recycling rates due to an increase in carbon burial and sedimentation due to a lower input of labile organic matter (Stevenson and Abbott, 2019). Increased fishing pressure is also likely to affect seafloor properties and topography (Palanques et al., 2001; Puig et al., 2012), thus leading to shifts in physically-driven DM and PM exchange processes such as resuspension and advective fluxes.

To test whether a shift in the position of the Polar Front and ongoing reduction in the annual duration of sea ice cover is likely to cause a change in benthic-pelagic fluxes in the region, a north-south transect through the Barents Sea was investigated which included stations substantially north and south of the current Polar Front. The location was determined to be ideal as the average annual sea ice cover duration across the stations covered a wide range, providing a proxy for current and likely future conditions. Practical steps taken to test the above included: Characterising the physical, biogeochemical and biological environment along the transect using a combination of direct sampling and experimental treatments, then quantifying PM and DM B—P exchange drivers and processes and finally determining the most likely effects of the climate change-driven changes described above on B—P exchanges. We chose to perform resuspension experiments with annular flumes as this is the best way to test sediment cohesion and simulate current-induced particle and solute exchanges across the sediment-water boundary, which was necessary in order to assess overall exchange potentials. Broad multidisciplinary sampling and experimental regimes were chosen as the comprehensive and holistic data set captured through them could help to characterize even complex environmental process such as benthic-pelagic exchanges.

There have been past research efforts to define arctic downward flux of pelagic organic material and its effects on the benthic environment (e.g. Ambrose and Renaud, 1995; Grebmeier, 1993; Søreide et al., 2013; Tamelander et al., 2006). The objective addressed here, to assess a broad range of biogeochemical, physical and anthropogenic drivers of exchange and determine upward and downward DM and PM fluxes under current and future conditions by integrating the driver data sets, is a novel and more holistic contribution to the field.

## 2. Methods

### 2.1. Study area

The Barents Sea Polar Front is currently located in the southern and central Barents Sea (Fossheim et al., 2006; Oziel et al., 2016). It is primarily constrained by the steep topography in the west, but further east is increasingly influenced by seasonal and inter-annual variations in Atlantic water inflow, temperature and wind speed (Ellingsen et al., 2007; Ingvaldsen, 2005). In addition to the underlying long-term climate-driven warming, the Barents Sea climate fluctuates between a cold and a warm stable state in irregular inter-to multi-annual intervals. The two states are triggered through oceanic and atmospheric circulation variations (Ådlandsvik and Loeng, 1990; Ingvaldsen et al., 2004). The Atlantic-dominated waters to the south of the Polar Front are warmer ($> 3$ °C) and more weakly stratified than the Arctic influenced waters further north, where salinity is the leading order control on a more strongly stratified water column. (Olli et al., 2002; Reigstad et al., 2002). Climate-driven reduction in seasonal sea ice cover is faster and more extreme in the Barents Sea than in other Arctic regions (IPCC, 2019; Onarheim et al., 2018), with some models predicting it to be completely free of ice year-round by 2080 (Furevik et al., 2002). While some studies state that sea ice cover can have an effect on deep water tidal flow in this area and vice versa (Aagaard et al., 1981; Ferrari et al., 2014; Kowalik and Proshutinsky, 1994), others discount ice influence below surface waters (Gjevik et al., 1994). The stations (B13 – B17, see Fig. 1) cover varying water mass distributions and typical durations and concentrations of seasonal sea ice cover from south to north.

The mean position of the oceanographic Polar Front in surface waters intersects the transect north of station B14 (Fig. 1, green dotted line; Fossheim et al., 2006; Stevenson and Abbott, 2019). The benthic Polar Front on the other hand, determined based on the divide between Arctic- and boreal-dominated benthic megafauna community composition, intersects nearer B13 (Fig. 1, red dotted line; Jørgensen et al., 2015). All stations were selected to be in areas of comparable depth (see Table 1) and sampling was carried out in July 2018 (Solan, 2018) and 2019 (Barnes et al., 2019), except the bioturbation and Bioirrigation measurements, which were made in July 2017 and 2018 (Hopkins et al., 2018; Solan, 2018).

Although the winter sea ice extent varies between years, the furthest south the ice edge typically reaches is 76°N (Onarheim and Årthun, 2017). B17 has a lower decadal average percentage of sea ice cover than B16 (see Table 1), even though it is further north, because warm Atlantic water also enters the Arctic basin via the Fram Strait and crosses the shelf break to the north of Svalbård where it frequently creates an ice free area north of the archipelago that can reach as far east as station B17 (Loeng, 1991; Loeng et al., 1997). Each of the stations was located in a glacial trough containing postglacial glaciomarine / marine trough-fill (Vorren et al., 1989), in the form of fine-grained cohesive sediments. Seafloor topography on the Barents Sea continental shelf, though dominated at large scales by the troughs themselves, also exhibits a range of trawling and iceberg plough marks (Thorsnes et al., 2016). Anthropogenic impacts on the benthic environment have been recorded even in areas that are covered by sea ice for the majority of the year and are thought to account for much of the small-scale seafloor variability (Sswat et al., 2015). Water mass transport and exchange across the shelf is guided by the bathymetry of troughs and banks (Pfirman et al., 1994) and has been shown to be variable on a seasonal as well as inter-annual basis (Loeng et al., 1997). The dominant current directions are an eastward flow in the southern Barents Sea and a westward flow in the north (Ellingsen et al., 2007). Tidal flow is also an important hydrodynamic force, that can induce turbulent mixing near the seabed (Rippeth

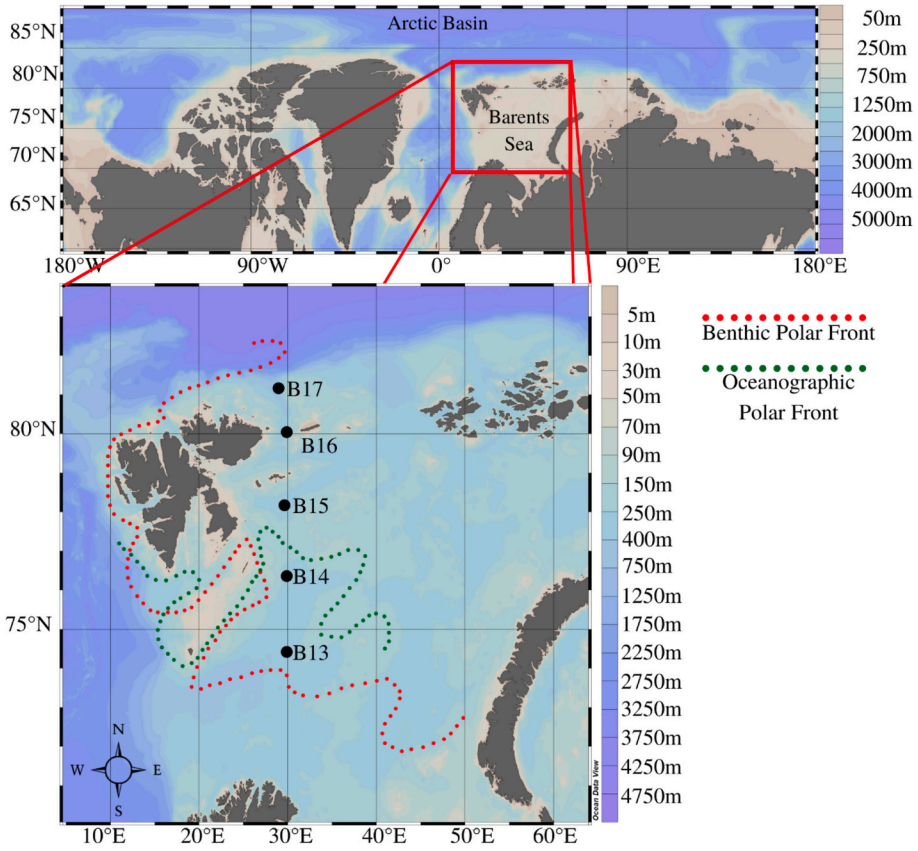


**Fig. 1.** Map of benthic stations B13, B14, B15, B16and B17 along the 30° longitudinal line east of the main Svalbård archipelago. Dark green dotted line indicates the typical location of the oceanographic Polar Front after Fossheim et al. (2006) and Stevenson and Abbott (2019); the dotted red line indicates the typical location of the benthic Polar Front after Jørgensen et al. (2015). (For interpretation of the references to colour in this figure legend, the reader is referred to the web version of this article.)

**Table 1**
Additional information on transect stations. Sample station locations and approximate depths (± 2.9 m on average, see appended Table A.1). Annual average sea ice cover percentages based on 2009 to 2019, as well as for 2018 and 2019 specifically, calculated from sea ice data provided by the Norwegian Meteorological Institute in grid boxes ±1°N and ± 1°E of each station (Norwegian Meteorological Institute, 2020).

| Station | Latitude | Longitude | Depth (m) | Average sea ice cover | | |
|---|---|---|---|---|---|---|
| | | | | 2009–2019 | Only 2018 | Only 2019 |
| B13 | 74.30°N | 30.00°E | 358 | 0 % | 0 % | 0 % |
| B14 | 76.30°N | 30.30°E | 292 | 6.18 % (+ – sd 6.96) | 6.03 % | 23.01 % |
| B15 | 78.15°N | 29.59°E | 313 | 53.68 % (+ – sd 12.27) | 42.19 % | 69.59 % |
| B16 | 80.07°N | 30.04°E | 280 | 63.75 % (+ – sd 22.52) | 43.01 % | 90.14 % |
| B17 | 81.16°N | 29.19°E | 334 | 62.52 % (+ – sd 25.23) | 30.14 % | 95.62 % |

et al., 2017; Sundfjord et al., 2007). Tidal currents are spatially variable in direction and magnitude throughout the Barents Sea and can be enhanced locally by topographic features (Kowalik and Proshutinsky, 1995; Le Fouest et al., 2011; Sundfjord et al., 2007).

The seabed at sampling stations chosen for this study is typically inhabited by a range of invertebrate epi-benthic and macro- and meiofauna (Cochrane et al., 2012). Their community composition has been shown to be impacted by natural as well as anthropogenic influences (see e.g. Denisenko et al., 2003; Jørgensen et al., 2019). Considering the depth of the water, fine-grained nature of the sediment and generally low current velocities, bioturbation has been estimated to be more important for internal sediment mixing than abiotic drivers (Maiti et al., 2010). Although the majority of local benthic macrofauna are surface or subsurface deposit feeders, low-intensity sediment mixing to shallow mixed depths does take place (Carroll et al., 2008a). Within the Barents Sea, areas of seafloor depression such as glacial troughs exhibit the lowest infaunal taxon richness and biomass, but the deepest biogenic sediment mixing depths of any habitat type (Cochrane et al., 2012). Because the glacial troughs are specialised environments and spatial variation of the seafloor throughout the Barents Sea is substantial (Norges Geologiske Undersøkelse, 2020), the results of this study are representative of these trough environments, not of the shelf as a whole. It should be said however, that glacial troughs are the primary characteristic of the Barents Sea topography (Faleide et al., 1996; Vorren et al., 1989), and that they are an important factor in Atlantic water flow across the shelf (Schauer et al., 2002).

During the current study, the location of the pelagic Polar Front was confirmed through conductivity, temperature and density (CTD) measurements to be roughly around the middle of the study transect at the time of sampling (between B14 and B15), so around the mean oceanographic Polar Front location (Fig. 1; Fossheim et al., 2006). Weather conditions during both cruises were calm with little wind, only minor wave activity and an abundance of fog. The extent of sea ice cover varied substantially between the two years of sampling (see appended Fig. B.1).

During the first cruise in July and August 2018, five stations along the 30° eastern latitude were sampled (B13 – B17; see appended Tables A.1, C.1 and D.1) while during the 2019 cruise only four of the stations could be sampled (B13 – B16; see appended Tables A.1, C.1 and D.1), due to the density and thickness of ice around B17. Station B15, while enclosed in very close drift ice at the beginning of the 2019 cruise,

was ice-free at the time of sampling five days later (see appended Table D.1, for dates and times of sampling at each station).

### 2.2. Sampling methods

Sediment samples were taken with a 0.25 $m^2$ USNL (United States Naval Laboratory) box corer by randomly selecting five sites within a 200 $m^2$ area surrounding the central location of each sampling station. *Re*-sampling of any single point was avoided through tracked drift within the area in a randomised direction, oriented on current and wind directions (see appended Table C.1, for average distances between replicate cores at each station in both years).

From each corer box, a 30 cm diameter round sub-corer, made of sections of a large PVC pipe, was used to extract an intact sediment core and the overlying water. Although the mechanics of a box corer do not guarantee that this water was in fact from near-benthic depths, using only those cores that had retained water guaranteed at least that there were no cracks in the sediment matrix allowing it to drain and wash away the top-most surface sediment. Immediately after extraction, sub-cores were transported into a temperature controlled (CT) laboratory, which was kept at the ambient bottom temperature of each station as determined by the CTD profiling preceding the sediment sampling where possible (see cruise reports in Solan, 2018 and Barnes et al., 2019), and at 2 °C in cases when further cooling was not physically possible (see appended table E.1 for true in-situ bottom temperatures measured via CTD at each station, CT room set temperatures, and CT room measured values). Disruption of the sediment matrix and accidental resuspension during core transport were avoided by using a carrying frame and rolling platform for core transport. Where the water level was insufficient upon taking the sub-cores, bottom water from CTD samples was used to replenish it using bubble wrap and airline tubing to minimise surface disturbance, as described by Widdows et al. (1998); see appended Table C.1 for CTD bottom water depths). Cores that surfaced without any water were rejected as the drainage of the overlying water may have removed the top-most sediment layer. Cores in which the sediment displayed cracks upon box-coring or sub-coring were also rejected. Each core was given a 24 h period between sampling and processing to settle, during which the water was aerated gently using diffusing air stones that did not disturb the sediment-water interface, and the cores were kept in the CT lab, in the dark.

Granulometry samples were taken from three to five of the USNL box cores at each station using 50 ml syringe corers. From each box core, three depth-integrated (0 to 5 cm sediment depth) syringe cores were extracted, combined and homogenised for subsequent sub-sampling during the analysis (see sampling details in Solan, 2018 and Barnes et al., 2019).

### 2.3. Ship-board in-situ data collection and sediment resuspension experiments

Sediment resuspension experiments were based on the Core Mini Flume (CMF) methods described in Thompson et al. (2013), using the 30 cm sub-cores, and carried out within the CT room. In essence, the CMF was inserted into the sediment core from above, thus creating an annular flow channel in which the CMF's motorized paddles could create a current (see image in Barnes et al., 2019). The flume was post-calibrated with a side-looking Nortek Vectrino Acoustic Doppler Velocimeter (ADV) as described in Thompson et al. (2013), positioned roughly 2–3 cm above the sediment core surface at each station. Areas outside of the channel were used for reference samples, providing data on conditions of the same core without flume impacts. The crossing of the threshold at which the sediment begins to be eroded and resuspension occurs was determined by gradually increasing the flow-speed, while recording optical backscatter and taking water samples at each speed step. The water samples were used to measure suspended particulate matter (SPM) and nutrients (nitrite, nitrate, ammonia, phosphate and silicate). SPM was sampled using a 50 ml Swinnex syringe filter system with pre–ashed (450 °C for 24 h) pre-weighed 25 mm Glass Fibre Filters (Whatmann). SPM samples were taken before, and after the critical shear stress application, as well as immediately before the end of each velocity step. The exact quantity of filtered water was recorded and filters were frozen at −20 °C for later analysis. Throughout the flume run, the overlying water was also sampled for nutrients (nitrate + nitrite, nitrite, ammonium, phosphate and silicic acid) by taking 30 ml samples at the same intervals as the SPM samples. Nutrient samples were filtered through acrodisk® supor® membrane filters (0.8 / 0.2 μm; VWR) and refrigerated until analysis, which was carried out within 24 h of sampling using a Lachat Quikchem 8500 flow injection analyser (Hach US, 2020; see methods detailed in Solan, 2018). Flux rates were based on the concentrations measured before the start of the resuspension experiment, which were considered a 0-level. A growing concentration with increased flow velocity was taken to indicate influx of nutrients from the sediment and pore water into the overlying water, and a lessened concentration indicated the opposite.

In addition to the water samples detailed above, sediment property measurements were undertaken representative of conditions before and after critical shear stress application. This was done by syringe coring sediment from areas which remained untouched by the resuspension (pre-resuspension, sampled in the same core but outside of the flow channel), and those within the flume channel (post-resuspension). The syringe cores were frozen and stored vertically, then sliced into sections of 0–1, 1–2, 2–3, and 3–5 cm depth from the sediment surface. Both SPM filters and sediment property samples were weighed wet, then dried in an oven in pre-weighed petri dishes over night at 60 °C and weighed again. To determine organic matter (OM) contents of both sediment and SPM, samples were then placed in a furnace and ashed for 24 h at 450 °C, after which they were weighed a final time to determine the amount of organic matter lost on ignition, which is given as a weight in g, per each cm of the syringe cores. Sediment porosity was calculated using the wet-dry method described in Maiti et al. (2010). Dry sediment density was calculated by weighing each 1 cm slice of the syringe cores after drying. Erosion depths were calculated based on the SPM volume placed in suspension throughout the flume run per volume of water, divided by the surface area of sediment within the flume, factoring in pre-resuspension sediment densities.

Granulometry samples were analysed using a Laser Coulter Sizer LS 130 micro volume model (Coulter International Corporation, 1996). Each replicate was sub-sampled five times and analysed, leading to a total of 15–25 measurements per station for each year. From this, the averages were used to determine depth-averaged grain size distributions. Median grain size (in the form of the particle diameter at 50 % in the cumulative distribution, known as $d_{50}$) values of each of the stations were used to calculate critical erosion velocities and shear stresses, following the methods outlined in Thompson et al. (2013), using power laws described in Soulsby (1997); see Eqs. (A) and (B)).

$$u_{*crit} = 0.121\left(d_{50}/z\right)^{1/7} U_z \tag{A}$$

$$\tau_{0crit} = \rho {u_{*crit}}^2 \tag{B}$$

$u_{*crit}$ = the critical erosion velocity (m $s^{-1}$) at which the sediment starts breaking down and particulates are resuspended, $z$ = the height above the seabed (m) at which the velocity measurement is taken, $U_z$ = the velocity (m $s^{-1}$) at height $z$ equal to the in-flume height of the acoustic doppler velocimeter with which the flume was calibrated, $\tau_{0crit}$ = the critical shear stress (Pa) meaning the force required to induce sediment erosion, and $\rho$ = the fluid density (kg $m^{-3}$).

In-situ current measurements were acquired to determine whether naturally occurring flow speeds would likely be able to cause sediment resuspension. During the 2019 cruise, a 75 kHz RD Ocean Surveyor Acoustic Doppler Current Profiler (ADCP) fitted to the ship's hull

provided profiles of horizontal current velocities, from approximately 20 m below the sea surface, to 20 m above the sea floor. Raw data were collected in 8 m water depth bins in a narrowband water tracking mode using RD VmDas software. Velocities close to the bottom that were contaminated by strong reflections from the seafloor were discarded. Following the processing and quality control procedures detailed in Souster et al. (2020), 10-min average velocity profiles were created, and the absolute water velocities were determined using the ships GPS derived velocity. Depth-mean velocities comprising the barotropic tidal velocity and any non-tidal contribution to the depth average flow (e.g. a density-driven geostrophic current) were calculated. The ship worked at each site for 30–48 h, therefore between 2.5 and 4 semi-diurnal tidal excursions were resolved each time. ADCP data were not collected in 2018 due to technical issues.

Although there are wind and density driven components to the circulation within the Barents Sea, most of the near bed variability in current speeds at the study sites is likely to be associated with oscillatory tidal currents. Therefore, for both cruise periods in 2018 and 2019, tidal current predictions were generated at each site using the Oregon State University (OSU) Tidal Prediction Software and the 2018 regional 5 km Arctic Ocean Tidal Inverse Model, AOTIM-5 (Egbert and Erofeeva, 2002; Padman and Erofeeva, 2004). Predictions were based on twelve harmonic constituents (including M2, S2, N2 and K2). They provide an estimate of the spring-neap range in velocities that each study site is likely to experience.

Sediment erosion and deposition are largely controlled by currents and shear stresses near the seabed. Friction at the seafloor creates a benthic boundary layer, within which currents increase logarithmically with height above the seabed towards free-stream velocities (Soulsby, 1997). Although it is known that bottom-friction reduces flow speeds near the seabed, there may be more vertical shear through the resulting turbulence (Richards, 1990). Thus, estimates of near-bottom velocities were derived from the depth-average currents (both the tidal predictions and observations) and the boundary roughness. The boundary roughness range, as determined following the recommendations in Soulsby (1997) for the combination of deep water and fine-grained sediment, suggests that near bed velocities should be estimated using Eq. (C), in which $\overline{U}$ = depth-averaged current speed (m $s^{-1}$) and $h$ = water depth (m; Soulsby, 1997; see Eq. (C) below).

$$U_{(z)} = \left(\frac{z}{0.32h}\right)^{1/7}\overline{U} \quad \text{(C)}$$

Near-bottom velocities thus derived ($\leq$ 0.12 m above the sea floor) were then compared with critical shear stresses measured at each station to determine whether typical near-bed current speeds at each site could cause seafloor resuspension events.

### 2.4. Supplementary data collection

Other parameters collected during the same cruises were used to supplement the data set (see cruise reports: Solan, 2018; Barnes et al., 2019). Benthic macrofauna (fauna >0.5 mm) biomass and abundance were recorded at all stations from 5 replicate UNSL box cores, that were sieved through a 0.5 mm sieve, in 2017, 2018 and 2019 (Barnes et al., 2019; Hopkins et al., 2018; Solan, 2018) and manually identified and weighed to determine species abundances, diversity and biomass. Bioturbation estimates based on mean and maximum mixed sediment depths, surface boundary roughness and biodiffusion coefficients (the latter is calculated based on biomass, abundance, mobility and sediment reworking traits, and measured on a unit-less scale; see Queirós et al., 2013), as well as bioirrigation measurements recorded by Solan et al. (2020) were included to gain an understanding of the biological activity at each of the sites. Bioturbation was measured by using luminophore tracers that were added to tanks containing intact macrofaunal communities from each station (collected vie USNL box corer), and recording the changes in luminophore distribution over the course of 12 days (see Hopkins et al., 2018). Bioirrigation was measured in the same experimental tanks, by recording the change in concentration of a Sodium Bromide tracer between the start and the end of the experimental period. Both of these data sets were collected at the same stations that are investigated in this study, but during the 2017 and 2018 cruises instead of 2018 and 2019, as in 2019 these data were not collected. Sea ice and water mass conditions in 2017 and 2019 were similar, justifying the use of the 2017 data on benthic biological activity as a proxy for ice-covered conditions here (Hopkins et al., 2018; Solan, 2018).

Information on potential bio-stabilisation of the sediment through biological means and benthic extracellular polymeric substance (EPS) production was available through personal communications and insights into unpublished data sets on sedimentary pigment composition and degradation, and water column transparent exopolymer particle (TEP) concentration data. They were collected throughout the 2018 and 2019 cruises during which this study's samples were taken (Barnes et al., 2019; Solan, 2018).

Localised sea ice cover duration data were provided by the Norwegian Meteorological Institute (Norwegian Meteorological Institute, 2020) and supplemental data on the sea ice extent between 2006 and 2017 were sourced from the Environmental monitoring of Svalbård and Jan Mayen platform (MOSJ, 2020).

An estimation of fishing pressure was collated using landings data exported from the ICES data set collections (ICES, 2020) as well as fishing effort data based on automatic identification systems (AIS; Global Fishing Watch, 2020). As trawling is the most likely fishing technique to impact the B—P interactions (Puig et al., 2012), information on trawling activity was isolated in the AIS data. As the algorithms currently used by Global Fishing Watch do not differentiate between different types of trawlers (bottom and mid-water), the trawling impact on seafloor environments based on these data may be over-estimated. AIS data were extracted from grid boxes surrounding each of the station's locations measuring an extra 0.01° latitude north and south, and an extra 1° longitude east and west.

The longitudinally elongated grid box shape was chosen due to this study's focus on the north-south gradient in water mass distribution and sea ice cover. Using these data, typical local annual fishing effort was estimated based on averages over the seven year period for which data were available for (2012–2018).

### 2.5. Statistical data analysis

To test whether a reduction in sea ice cover duration and northward shift of the Polar Front could lead to changes in B—P exchange processes, seafloor and water flow properties had to be characterized, to provide context. Sedimentary conditions along the transect were characterized in both ice free and ice-covered conditions. In the contextual characterisation of the benthic environment, Analysis of Similarity tests (ANOSIM; cran R vegan package, Oksanen et al., 2019) were chosen to check for differences between the five stations as well as the two years, using 2-way designs on Euclidean distance matrices of the data, due to their flexibility in within-group as well as between-group testing. Another reason for this choice was the highly diverse nature of the data set (a range of variables recorded in different units and orders of magnitude), promoting the use of ranked dissimilarity matrices over analyses of the raw data. Predictors for ANOSIM testing were the two

years of sampling, the sampled stations, and a selection of sampled stations divided into those north of, and those south of the Polar Front, respectively. Response variables were the environmental variables investigated in each of the reported ANOSIM tests. To satisfy the conditions of ANOSIM testing, data were pre-screened for heteroscedasticity between groups via Breusch-Pagan testing (Breusch and Pagan, 1979) and found to be satisfactorily homoscedastic in all cases. Samples taken across a range of time points (e.g. throughout a resuspension cycle) or along sedimentary depth profiles were also tested for differences between time points and/or depths using ANOSIM. Correlation analyses between sea ice extent and fishing effort between 2006 and 2017 and 2012 and 2016 were carried out, using landings and AIS data respectively as a proxy for trawling. Data that displayed normal distributions were tested using parametric correlation analysis (Pearson, 1895) and non-normally distributed data were tested using non-parametric correlation (Spearman, 1904). Critical erosion thresholds determined through experimental flow channel measurements were compared against predicted tidal current speeds and directly measured current velocities to reveal the effects of physically driven exchange processes through frictional stresses on the seabed.

Processes were broken down into the categories identified in Rühl et al. (2020b): PM exchanges in 1) deposition, 2) resuspension and 3) overall flux, and DM exchanges driven by 1) advection, 2) physical resuspension, 3) biological mixing, 4) bioirrigation, and 5) diffusive flux. In order to quantify B—P exchange potentials of DM and PM within their individual driver groups as well as those of the exchange processes themselves at each station in both years, variables were combined into a variety of data sub-sets for different parts of the analysis. OM flux was used as an example of particulate B—P exchange and phosphate and silicic acid fluxes were used as examples for solute exchange. To investigate individual B—P exchange drivers or processes, biological, physical and chemical variables likely to impact the exchange were selectively included based on relationships identified in Rühl et al. (2020b). The choice or parameters included in assessing each of the exchange processes are indicated in Table 2 through tick-marks by each relevant driver.

Data sets were normalized using z-scoring, to account for differences in scale and units between variables. To avoid an over-estimation of the impact of variables that are interdependent or derived from one another (e.g. $\tau_0$ is partially derived from $d_{50}$), factors considered to be affected by this impact were selectively excluded. This was done based on where strong inter-variable dependencies were found through the calculation of a correlation matrix of all variables followed by individual assessment of derivative relationships between variables with strong correlations. For example, where both $\tau_0$ and $d_{50}$ were considered of importance, $d_{50}$ was excluded as a separate factor as it was already considered through the inclusion of $\tau_0$. Factors that were excluded from models through these considerations are indicated by parentheses around their ticks in Table 2.

To quantify B—P exchange drivers and processes and to determine cause-effect relationships between the two as well as to individual environmental variables, the sub-group defined in Table 2 were analysed using orthogonal partial least squares (OPLS) analyses (as introduced in Rühl et al., 2020a; Thévenot et al., 2015). OPLS were chosen due to their suitability for between-class discrimination when large within-class variation may be present, and to allow incorporation of the various data sets to equal degrees (Bylesjö et al., 2006). Within the OPLS, the individual stations and the north / south (ice / no ice) divide were applied as the classes by which to group the data. Variable Influence on Projection (VIP) values >1 identified factors contributing significantly to the model fit. VIP values reflect loading weights of each model components as well as quantifying the variability of the response explained by the components (Mehmood et al., 2012).

The contextual information provided through the previous analyses paints a vivid picture of the conditions at the seafloor-water boundary in areas representing the current, ice-covered, Arctic as well as future ice-

**Table 2**
Selection of driving factors for each direct driver of DM and PM exchange, as well as the overall exchange processes; Variables in parentheses denote selective exclusion of these variables from some tests, to avoid over-weighting them as they are already represented within other variables (see in-text explanation).

| Process | Driving variables | | | | | | | | | | | | | |
|---|---|---|---|---|---|---|---|---|---|---|---|---|---|---|
| | $d_{50}$ | $\tau_0$ | Sediment density | Sediment TOM concentration | Sediment porosity | Phosphate and silicic acid concentration | Phosphate and silicic acid fluxes | SPM and suspended OM concentration | SPM and suspended OM flux | Bioturbation (depth and surface boundary roughness) | Bioirrigation (biodiffusion coefficient and Bromide tracer flux) | Max. current velocity | Estimated trawling effort |
| PM Resuspension | (✓) | ✓ | ✓ | ✓ | | | | | ✓ | ✓ | | ✓ | ✓ |
| PM Deposition | | | | | | | | ✓ | | | | ✓ | |
| Absolute PM flux | (✓) | ✓ | ✓ | ✓ | | | | ✓ | ✓ | ✓ | | ✓ | ✓ |
| Diffusion-driven DM exchange | | | | | ✓ | ✓ | | | | | | | |
| Phys. Resuspension driven DM exchange | (✓) | ✓ | ✓ | | | (✓) | ✓ | | | ✓ | | ✓ | ✓ |
| Advection-driven DM exchange | (✓) | ✓ | | | ✓ | (✓) | ✓ | | | | | ✓ | |
| Biological mixing driven DM exchange | | | | | | ✓ | | | | ✓ | | | |
| Bioirrigation-driven DM exchange | | | | | ✓ | ✓ | | | | | ✓ | | |
| Absolute DM flux | (✓) | ✓ | ✓ | | ✓ | (✓) | ✓ | | | ✓ | ✓ | ✓ | ✓ |

free conditions. Using this, a non-quantitative assessment of the effects of sea ice loss and Polar Front location shift on the direction and magnitude of B—P exchanges was made by taking into account the normalized values of each set of drivers of relevance to the individual DM and PM exchange pathways (as identified in Table 2). Factors driving upward fluxes were negative, and those driving downward fluxes were positive, enabling us to create an illustration of the overall directions at each station and their relative strengths by weighing up the upward and downward drivers against each other.

## 3. Results

### 3.1. In-situ B—P conditions

Critical shear stresses were significantly lower in 2018 than in 2019 at all stations except B14 (ANOSIM, $R = 0.38$, $p = 0.002$; see Fig. 2 top). The differences between stations within each year were not as distinct but still significant, with higher values at B14 and B15 and lower values at B16 and, in 2018, at B13 which is due to the corresponding differences in mean grain size (ANOSIM, $R = 0.198$, $p = 0.032$). Within-station dissimilarity was highest at B16 in 2018 and at B13 in 2019. Mean sedimentary grain size was smaller at the two northernmost stations than in the southern region in both years (2018: ANOSIM, $R = 0.221$, $p = 0.0001$; 2019: ANOSIM, $R = 0.21$, $p = 0.0003$; see Fig. 2 bottom).

There were also variations in volumetric size class distribution along the transect in both years, exhibiting a higher clay content in the north and more silt in the southern region (2018: ANOSIM, $R = 0.241$, $p = 0.001$; 2019: ANOSIM, $R = 0.216$, $p = 0.0007$; see appended Fig. F.1). There was no significant difference in dry sediment density between the different stations within year and sediment depth groups (ANOSIM, $R = -0.001$, $p = 0.57$) though, overall, dry sediment density was higher in 2019 than in 2018 (ANOSIM, $R = 0.544$, p = 0.0001; see Fig. 3). The level of variability in TOM content with depth was significant within each year and at each station (ANOSIM, $R = 0.464$, p = 0.0001; see Fig. 4 for depth distributions).

The effects of simulated resuspension on measured sediment density were most notable in 2019, leading to lower densities in the top 1 cm (ANOSIM, $R = 0.125$, $p = 0.036$). Sediment porosity was also overall higher and less similar in 2018 than in 2019 within station groups ($R = 1$, $p = 0.008$). Porosity varied with depth (ANOSIM, $R = 0.134$, $p = 0.0001$) and correlated to the variation of the sediment density (Pearson's, $t = -10.332$, df = 246, $p < 0.000001$; see Fig. 3). Overall total organic matter (TOM) content within the sediment (i.e. concentration) was higher in 2018 than in 2019 (ANOSIM, $R = 0.575$, p = 0.0001, see Fig. 4). Most inter-station variation was found within the 3–5 cm depth layer in 2019. Differences in TOM content between samples collected from the same cores before and after resuspension experiments were not statistically significant (2018: ANOSIM, $R = -0.077$, $p = 0.987$; 2019: ANOSIM, $R = -0.028$ $p = 0.65$). Sediment density and TOM content across all stations were not correlated in either year (2018: Pearson's, $t = -0.9773$, df = 142, $p = 0.3301$; 2019: Pearson's, $t = -0.36508$, df = 102, $p = 0.7158$). Erosion depths were deeper overall in 2018 than in 2019 ($R = 0.152$, $p = 0.009$, see horizontal lines in Fig. 4). They were however found to be independent of sediment grain size (Pearson's, $t = -1.5367$, $p = 0.1682$), 0–1 cm depth in-situ sediment density (Pearson's, $t = -0.2142$, $p = 0.8365$) and 0–1 cm depth in-situ sedimentary TOM content (Pearson's, $t = 1.5792$, $p = 0.1583$). Ambient levels of SPM and suspended OM prior to resuspension were higher in 2018 than in 2019. Throughout the in-flume shear stress application, the amount of SPM and suspended OM increased over time at all stations during both years (SPM: ANOSIM, $R = 0.851$, $p = 0.003$; OM: ANOSIM, $R = 0.812$, p = 0.003; see appended Fig. F.1). Ambient OM concentration, as measured within flumes after the 24 h settling period before the start of the resuspension experiments, in 2018 was highest at B13, followed by B15 and B17, and lowest at B16 and B14. While in 2018 ambient SPM levels were highest at B15, lower at B13 and B17 and lowest at B14 and B16, in 2019 the concentration of both SPM and OM was found to be highest at B13, decreasing continuously northwards along the transect. The concentration of suspended OM before and after resuspension showed no correlation with sedimentary TOM levels at the sediment surface (2018: Pearson's, $t = 0.40177$, df = 32, $p = 0.6905$; 2019: Pearson's, $t = 0.66749$, df = 24, $p = 0.5108$).

Shear stress-driven B—P flux rates of ammonium, phosphate, silicic acid and nitrite did not differ significantly between 2018 and 2019 on the whole (ANOSIM, $R = 0.131$, $p = 0.19$). Sediments in the area were a net source of phosphate and silicic acid but a net sink for nitrogen. Silicic acid and phosphate fluxes from the sediment into the water were initiated even at very low current speeds, below the respective critical erosion velocities (between 1.06 and 1.55 cm $s^{-1}$ in 2018 and between 0.13 and 0.79 cm $s^{-1}$ in 2019; see Fig. 5). Flux development was not uniform between stations, but generally followed the same trend (upward or downward) over the course of the experimental resuspension cycles.

The shear stress-driven increase in phosphate in the water column was highest in B14 and lowest at B15 in 2018, but highest at B15 and lowest at B16 in 2019, with significant inter-station differences in both years (ANOSIM, $R = 0.491$, p = 0.0001). Net silicic acid efflux was largest at B16 in 2018 and at B14 in 2019, and smallest at B14 in 2018 and at B16 in 2019 (ANOSIM, $R = 0.246$, $p = 0.017$).

Benthic macrofauna species assemblages varied along the transect, showing a clear difference between the southern (B13 and B14) and the northern stations (B16 and B17), with higher levels of biodiversity in the northern area (Solan et al., 2020; see also higher abundances in Fig. 6, top). Macrofauna abundance was higher at B16 than at the other stations (Fig. 6, top) and biomass was low with little variability in all years at B15 (Fig. 6, bottom). Dissimilarity in both biomass and abundance was significant between stations (ANOSIM, $R = 0.225$, $p = 0.0003$ and $R = 0.655$, p = 0.0001 respectively) but not between years with different levels of ice cover. The recorded taxa were consistent throughout the transect and across the years.

Bioturbation led to deeper mixing depths and rougher surface boundaries in ice free conditions than under ice cover (Fig. 7, top and middle), across the whole transect (ANOSIM, $R = 0.488$, $p = 0.0002$) but neither differed significantly between stations within each year (ANOSIM, $R = 0.05$, $p = 0.23$). Bioirrigation was similar at all stations in 2017 but in 2018 bioirrigation rates were higher at B13 than the rest of the stations (ANOSIM, $R = 0.211$, $p = 0.014$; see Fig. 7, bottom).

Sediment surface pigment concentrations varied along the transect

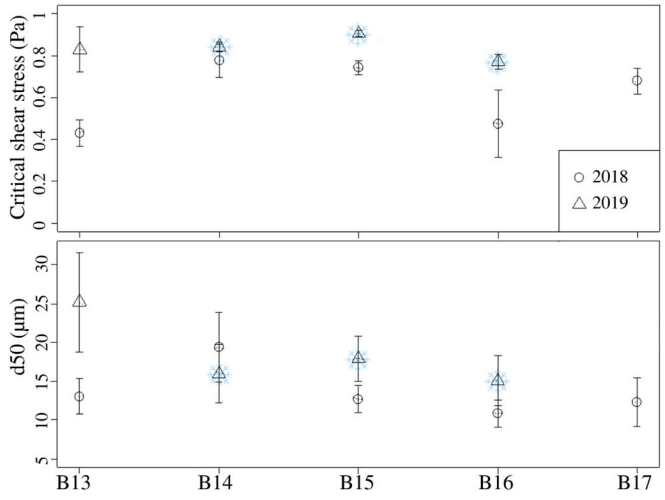


**Fig. 2.** Top: Critical shear stress at each station in 2018 and 2019; Bottom: Mean sedimentary grain size ($d_{50}$) at each of the stations in 2018 and 2019. Snowflake icons indicate sea ice presence at that stations in that year.

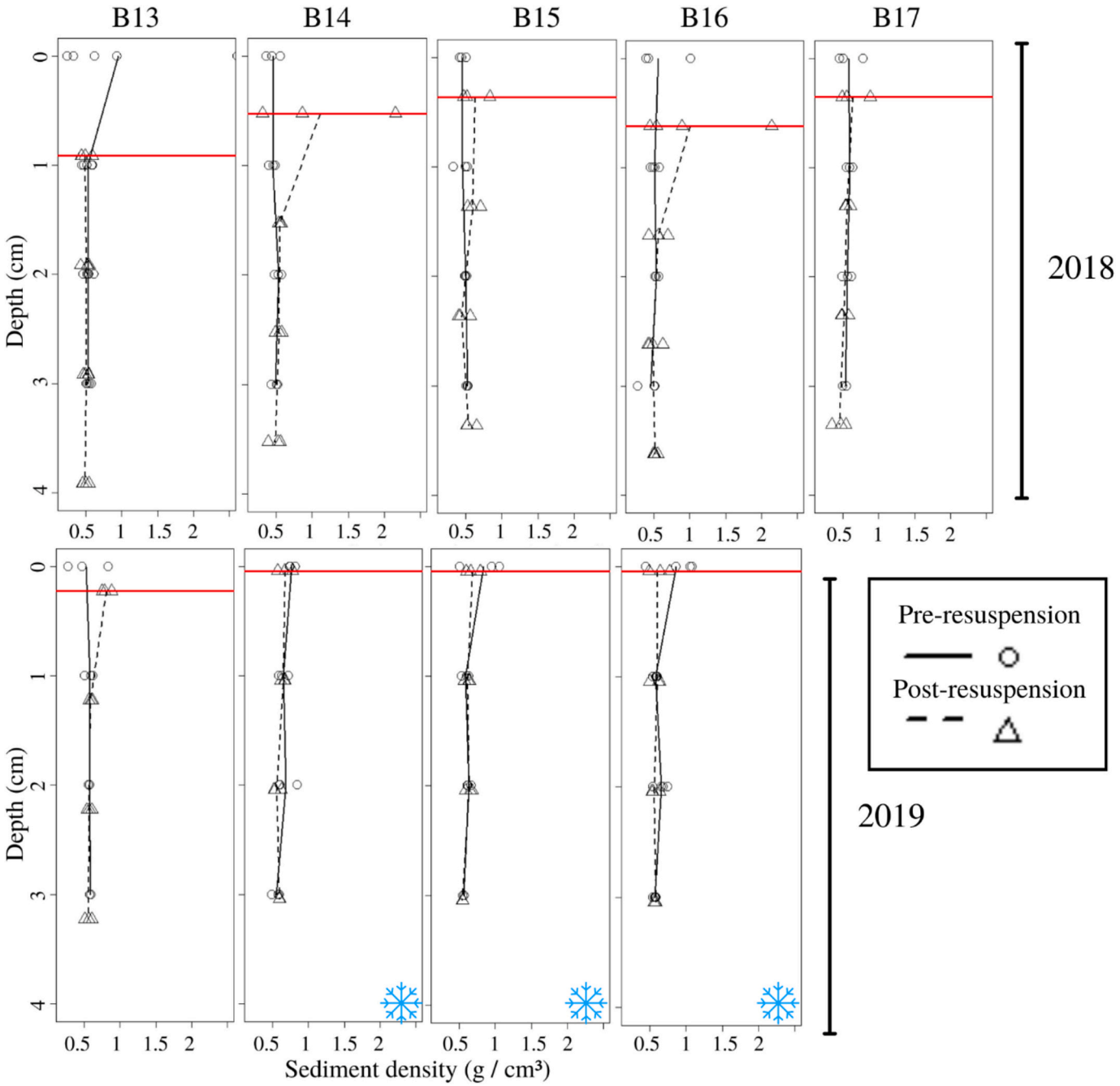


**Fig. 3.** Average dry sediment density. Before (continuous line, variability shown through plotting of replicate samples as circles) and after resuspension (dotted line, variability shown through plotting of replicate samples as triangles) at each station in 2018 (top row) and 2019 (bottom row). The red horizontal lines show the erosion depths, which are also the new sediment surfaces from which the sediment density depth profiles were measured after resuspension had taken place. Snowflake icons in the bottom right corners of the plots indicate sea ice presence at that stations in that year. (For interpretation of the references to colour in this figure legend, the reader is referred to the web version of this article.)

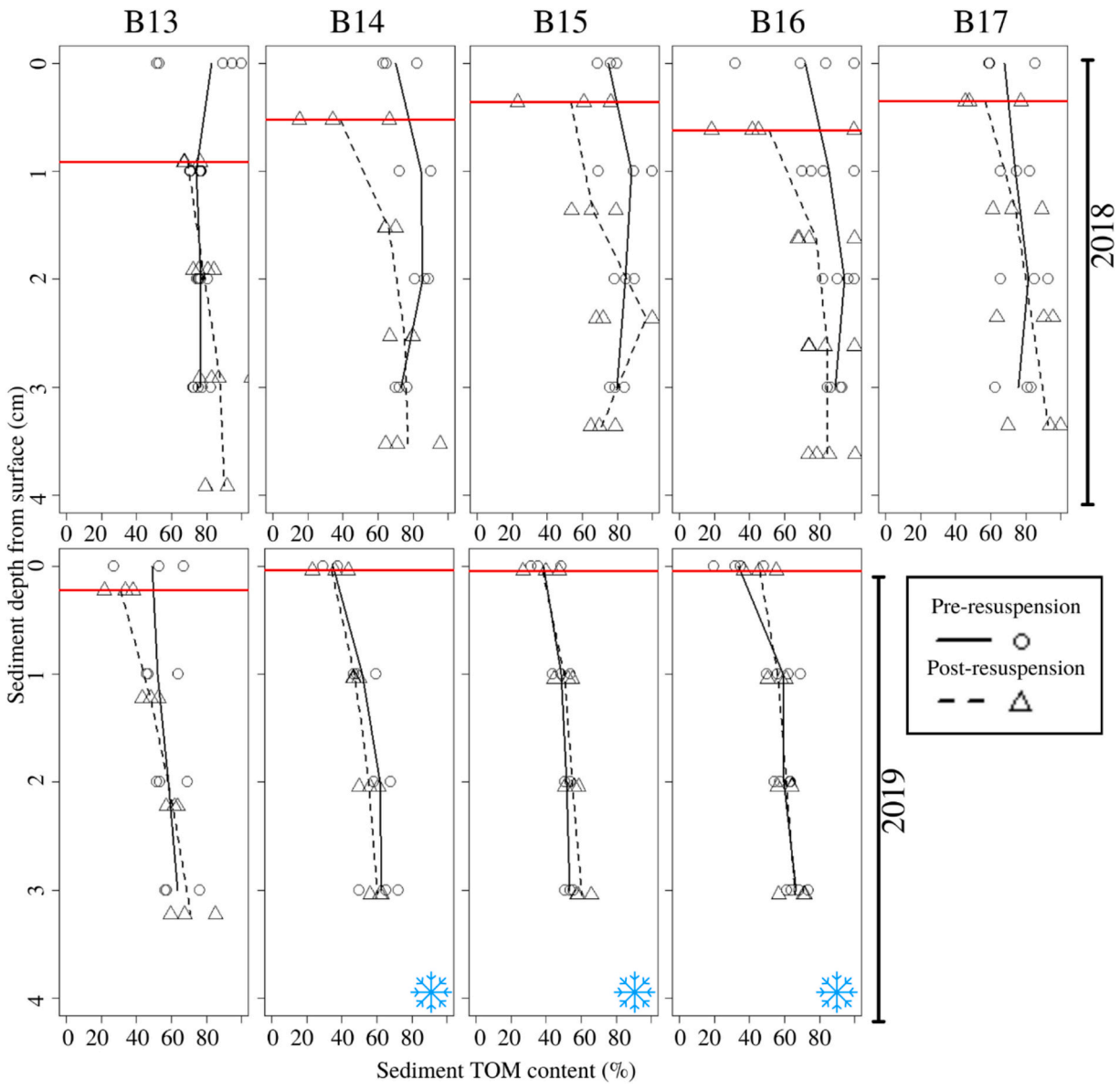


**Fig. 4.** Average sedimentary TOM content. Before (continuous line, variability shown through plotting of replicate samples as circles) and after resuspension (dotted line, variability shown through plotting of replicate samples as triangles) at each station in 2018 (top row) and 2019 (bottom row). The red horizontal lines shows the erosion depths, which were also the new sediment surfaces from which the sediment TOM content depth profiles were measured after resuspension had taken place. TOM was measured in g per cm of syringe core (see methods). Snowflake icons in the bottom right corners of the plots indicate sea ice presence at that stations in that year. (For interpretation of the references to colour in this figure legend, the reader is referred to the web version of this article.)

(see also Stevenson et al., 2023). Overall pigment concentrations peaked near the Polar Front in both ice-covered and ice free conditions, while the percentage of unaltered chlorophyll-*a* was highest at the station nearest the ice edge, so B17 and B14 in 2018 and 2019 respectively. Pigment samples taken at the sediment-water interface include both plankton and ice algae material, particularly in locations where the recent sea ice retreat would have caused a down-flux of algal organic matter (see also evidence based on these same data in Stevenson et al., 2023). TEP area per volume in near-bottom water was lowest at B14 near the Polar Front, with 4.46e+7 $mm^2$ / l, which constitutes roughly half as much as what was found at the other stations.

Tidally, east-west currents were dominant at B13 and B14 while north-south currents prevailed at the northern stations (see appended Fig. G.1). The tidal current regimes, one of the most influential factors on near-bed velocities, varied significantly between sites (see Fig. 8).

A strong, rectilinear tide (leading to a drop in slack tide velocities and associated shear stress to near zero every 6 h) was found at B16, resulting in estimated near bed velocities of nearly 7 cm / s at spring tides. In contrast, at B14 the tidal currents were weaker and more elliptical, and therefore a more constant near bed velocity of 2.5 cm / s was estimated. Comparing the observed depth-average currents in 2019 with the tidal current predictions suggests that at all sites there was an additional non-tidal velocity component of approximately 5 cm / s (see appended Fig. G.1), which equates to an additional 1.34 cm / s of flow

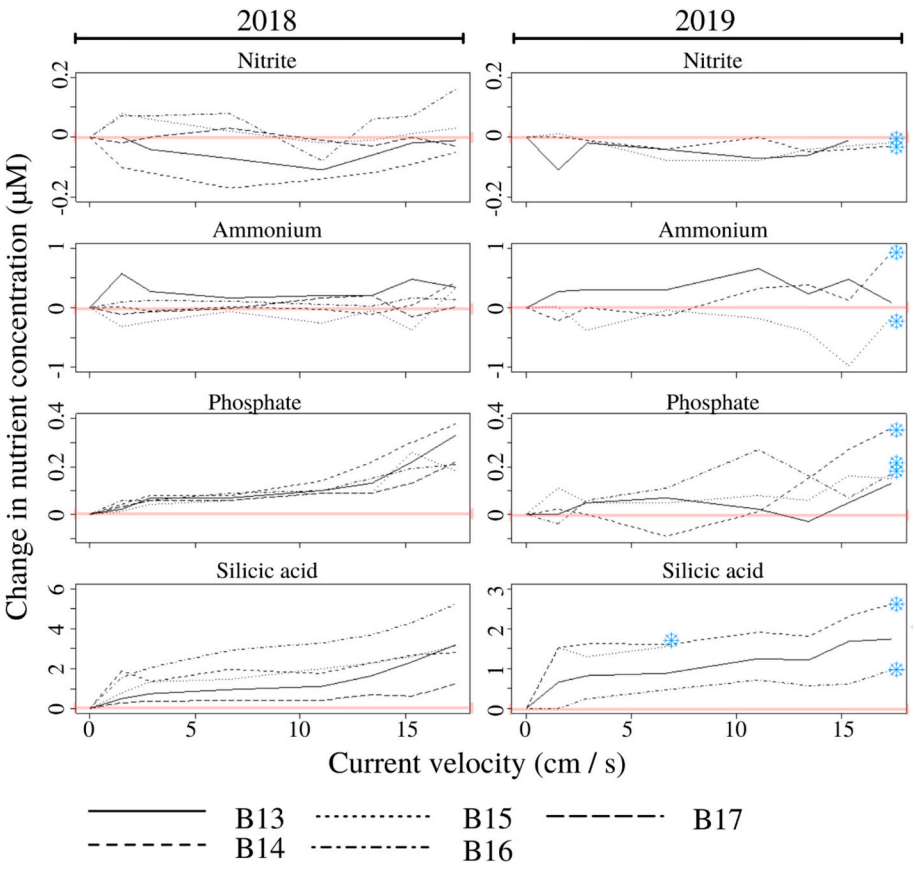


**Fig. 5.** Changes in nutrient concentration, driven by increasing current velocities during resuspension experiments, relative to stagnant concentrations in the flume cores' water (pre-resuspension; represented in the plots as the 0-line starting point). Snowflake icons indicate sea ice presence at that stations in that year.

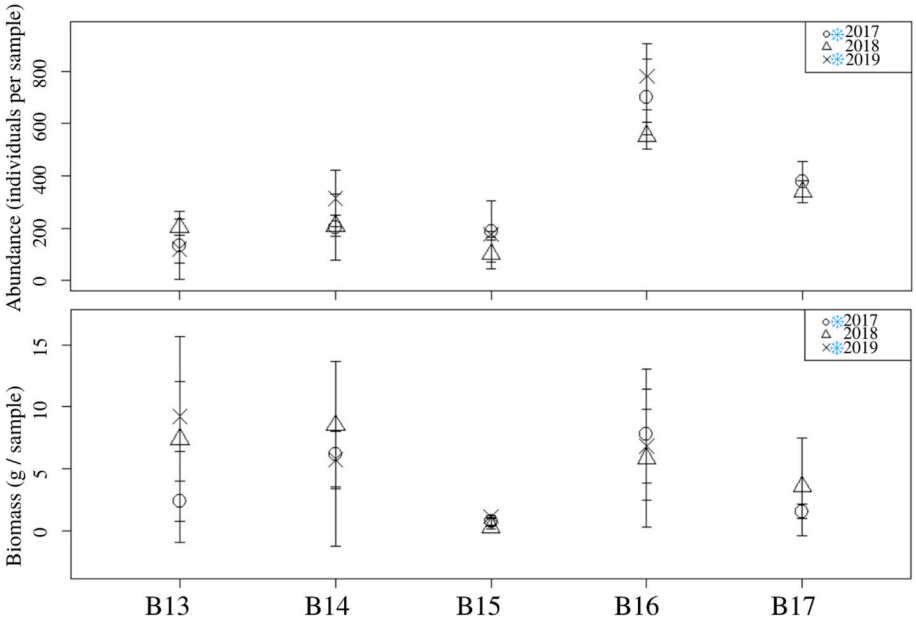


**Fig. 6.** Benthic macrofauna. Abundance (top) and biomass (bottom) at each of the stations in 2016 and 2017 (ice covered conditions) as well as 2018 (ice free conditions). Light blue snowflake icons in the legend indicate sea ice presence in those years from station B14 northwards. (For interpretation of the references to colour in this figure legend, the reader is referred to the web version of this article.)

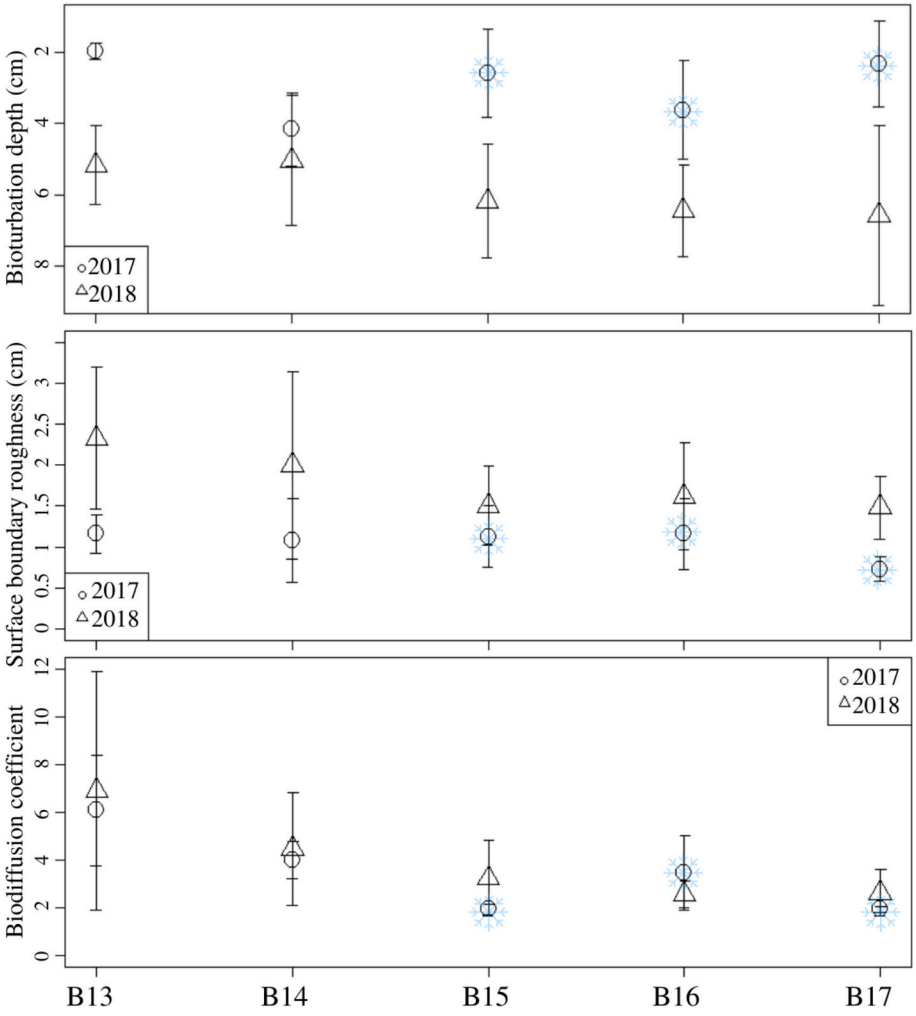


**Fig. 7.** Bioturbation. Bioturbation depth in cm (top), surface boundary roughness (middle) and biodiffusion coefficient (bottom) at each of the stations in both 2017 (ice covered conditions roughly equivalent to 2019) and 2018 (ice free conditions). The blue snowflake icons indicate sea ice presence at those stations in that year. (For interpretation of the references to colour in this figure legend, the reader is referred to the web version of this article.)

near the sea bed.

The differences between estimated near bed and critical erosion velocities shows that, with the possible exception of B16, at most sites velocities within the benthic boundary layer are unlikely to induce resuspension (see Figs. 9 and 10).

At B16 the near bed velocities estimated from the short ADCP record suggest that the critical erosion threshold can be exceeded, which may trigger advective and resuspension-driven B—P fluxes. Comparing the predicted tidal velocities with the ADCP measurements taken during the 2019 cruise shows that tidal currents can account for more than half of the flow speed at B13, B15 and B16, and almost all at B14 (see Fig. 9). In 2018, tidal currents were predicted to be sufficiently strong at B16 (and in some instances at B13 too, see error bars in Fig. 9) to cross the critical erosion point, and presumably trigger associated advective and resuspension-driven B—P fluxes. ADCP current measurements in 2019 show that in this year, overall current speeds at B16 were also high enough to drive such fluxes. The additional non-tidal components of the current velocities included in the ADCP estimates of 2019 showed residual east-ward flow of roughly 2 cm $s^{-1}$ at B13, residual south-east flow of 4–6 cm $s^{-1}$ at B14, north-west residuals of around 1 cm $s^{-1}$ at B15 and north-easterly residual flow of 1–1.5 cm $s^{-1}$ at B16. Each site was visited at a different point in the spring-neap cycle, and S—N range in tidal velocities differed between sites.

Sea ice cover in April, when the ice extent is on average at its maximum, was correlated with fish landings data (Pearson's, $t = 3.3124$, $p = 0.007847$), but September sea ice cover (least extensive on average) did not correlate to the landings data (Pearson's, $t = 0.14794$, $p = 0.8853$). Based on AIS data, the estimated average number of annual hours of trawling was highest at B13 (117.69 h) and lowest at B16 (0 h; see Table 3 for more detail). Estimated trawling hours were negatively correlated to percentage sea ice cover at the stations (Pearson's, $t = -4.3336$, $p = 0.0001293$) in this seven year period.

### 3.2. Overall B—P exchange of POM and nutrients

The following results are based on the non-quantitative flux estimations described in Section 2.5, designed to give an idea of direction and strength of the fluxes relative to location, but respective to DM and PM.

At the two southern, Atlantic-dominated, stations (B13 and B14) the

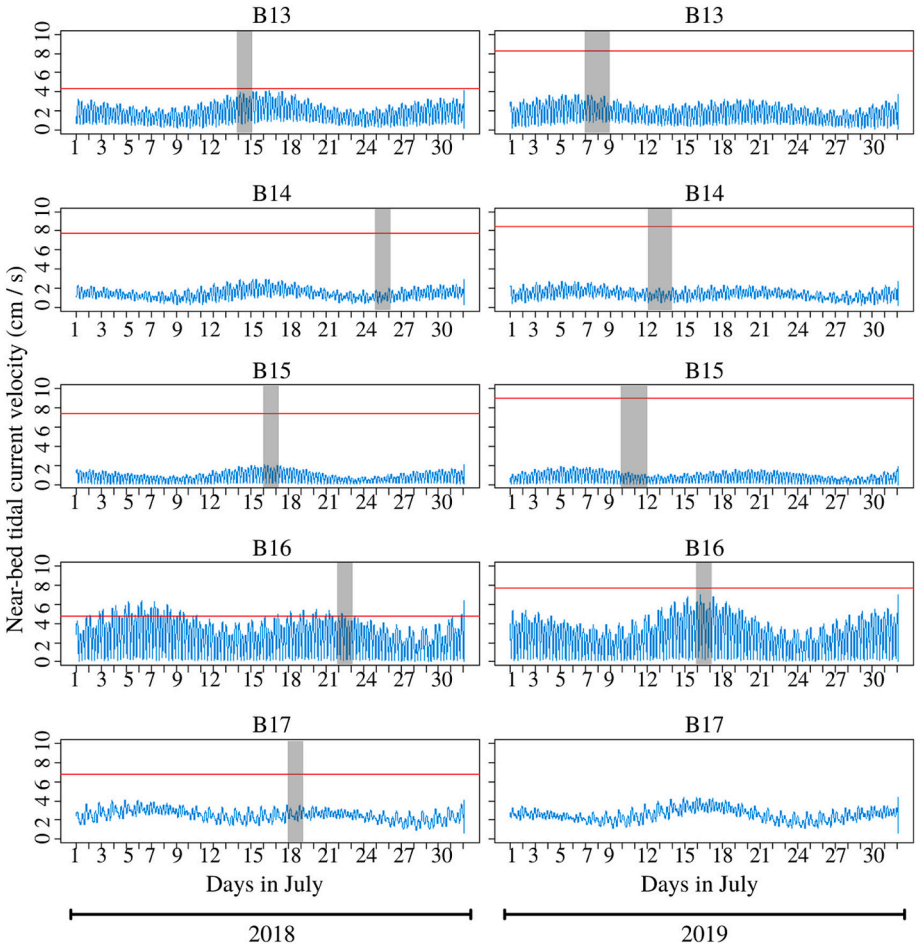


**Fig. 8.** Estimated near bed velocity. Velocity magnitude derived from tidal current predictions (cm / s), 2018 on the left, 2019 on the right; dates during which the stations were visited are marked in grey; critical erosion velocities for each location are marked by the horizontal red lines. (For interpretation of the references to colour in this figure legend, the reader is referred to the web version of this article.)

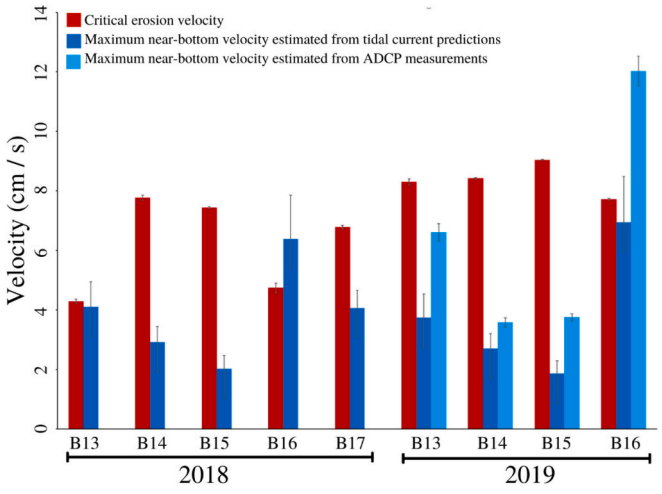


**Fig. 9.** Maximum near-bed velocity. Velocities in July 2018 and 2019 estimated from *barotropic tidal current predictions (using Eq. C); Maximum near-bed velocitystimated from the depth average currents recorded by the ADCP during on-site sampling in 2019 using Eq. C); and critical erosion velocities (see Eq. A) at each station in both years; error bars depict standard deviations.*

overall flux of DM (specifically of dissolved silicic acid and phosphate) was directed downward, from the pelagic towards the benthos. At the three Arctic-influenced stations on the other hand (B15-B17), DM fluxes were directed upward (See Fig. 10, top).

Though each individual station was not overall significantly different from the others in the inter-station OPLS model, it confirmed the 2-way grouping of southern (B13 and B14) and northern stations B15-B17 (Model 1, R2X = 0.535, R2Y = 0.93, Q2 = 0.604, pR2Y = 0.15, pQ2 = 0.1; see appended Table H.1, for VIP scores >1). Modelling the transect according to this latitudinal divide showed that there were distinct differences between the two groups (Model 2, R2X = 0.678, R2Y = 0.971, Q2 = 0.762, pR2Y = 0.1, pQ2 = 0.05). The split was attributable to differences in geophysical and biogeochemical parameters (sediment grain size, phosphate concentration and shear stress-driven phosphate flux), biological parameters (bioturbation depth and biodiffusion coefficient), and anthropogenic pressures (annual trawling hours spent at the sites estimated from AIS data; see appended Table H.1, Model 2 for all VIP scores >1). The relative importance of each of the driver groups towards these fluxes varied between the stations, though diffusion and advection-driven B—P exchanges were generally the most important, while the influence of physical resuspension was small across the whole transect, according to the OPLS results. Biological mixing had more impact on DM B—P exchanges than bioirrigation.

PM B—P exchanges (of organic and inorganic particulate material) were dominated by an upward flux at B13 and a downward flux at all other stations (see Fig. 10, bottom). Upward and downward transport of

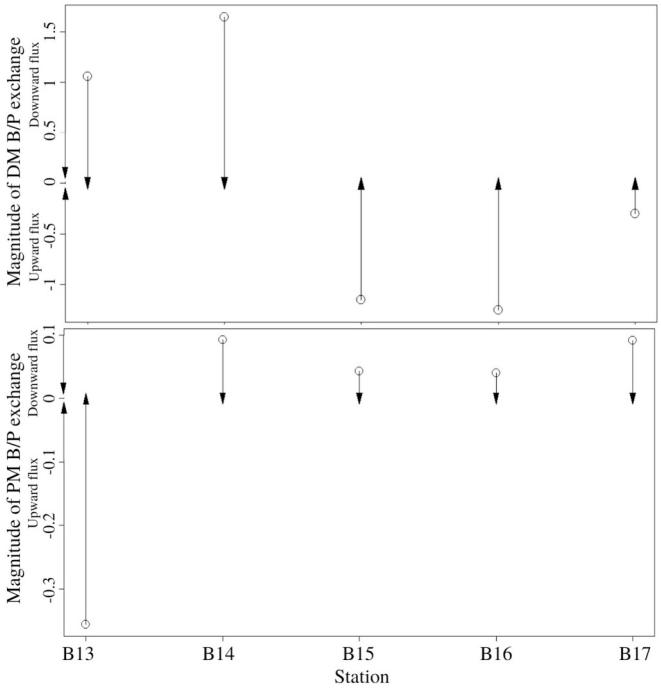


**Fig. 10.** Vertical dissolved and particulate matter exchanges. DM (top) and PM (bottom) B—P exchange potential at each of the stations.

**Table 3**
Annual trawling effort at each station. Trawl data estimations based on 2012–2018 AIS records within the grid boxes surrounding the sample stations as specified in the methods section. As no AIS data were available for 2019, it was impossible to determine whether the sites had been trawled in that year prior to sampling, especially at B13 and B14. Trawling events more recently than this are highly likely based on the seasonal timing of the trawling at these stations recorded in the other years.

| Station | Estimated average hours of trawling per year | Number of months during which site is trawled annually | Number of years in which site was trawled between 2012 and 2018 | Average number of trawling incidents per year (average, maximum and minimum) | Time since last estimated trawling incident at time of sampling | |
|---|---|---|---|---|---|---|
| | | | | | 2018 | 2019 |
| B13 | 117.69 (+ − sd70.09) | 1–6 (average 3.86) | 7 / 7 | 207.14 (max 666, min 46) | 16 days | 215 days (likely fewer) |
| B14 | 68.18 (+ − sd 79.47) | 1–5 (average 3) | 7 / 7 | 47.86 (max 128, min 6) | 59 days | 411 days (likely fewer) |
| B15 | 2.79 (+ − sd 2.83) | 1–3 (average 1.29) | 5 / 7 | 11 (max 38, min 1) | 273 days | 245 days |
| B16 | 0 | 0 | 0 / 7 | N / A | N / A | N / A |
| B17 | 0.69 (+ − sd 1.26) | 0–1 (average 0.29) | 2 / 7 | 2.5 (max 3, min 2) | 551 days | N / A |

particulate matter were roughly equally important at all sites except for B13, where upward fluxes were dominant. This more southerly bilateral divide was reflected in the inter-station OPLS model (Model 3, R2X = 0.594, R2Y = 0.824, Q2 = 0.606, pR2Y = 0.15, pQ2 = 0.1, see VIP scores >1 in appended Table H.1, Model 3). *Re*-modelling the division between B13 and the rest of the stations showed that differences in ambient SPM and suspended OC concentrations, biological activity and annual trawling hours were the main drivers of the latitudinal split (Model 4, R2X = 069, R2Y = 1, Q2 = 0.902, pR2Y = 0.05, pQ2 = 0.05; see VIP scores >1 in appended Table H.1, Model 4).

## 4. Discussion

The use of flume experiments to assess sediment erodibility and upward flux potentials is well established in the context of sediment dynamics studies, but the resulting assessment of ecosystem level B—P exchanges as detailed in this study is more novel. Flumes are more commonly used in intertidal environments that are more readily accessible (e.g. Ubertini et al., 2012) or in highly controlled but less complex laboratory and mesocosm set-ups (e.g. Egea et al., 2023). The strength of the current study lies in the combination of in-situ measurements and experimental data that collected on-site using freshly cored and intact sediment matrices, providing a holistic snapshot of the conditions.

We found that the overall potential for PM flux was much lower than that for DM flux, which suggests that DM B—P exchanges are of a greater magnitude and importance than PM exchanges on the Barents Sea shelf. A fundamental change in the exchange dynamic of either (DM or PM), and especially the combined effects of a change in both, could have wide-reaching consequences for the Barents Sea Ecosystem, such as shifts in the biological community composition and diversity. Factors driving the differences between the Atlantic-dominated and the Arctic-dominated stations can be split into direct and indirect drivers of B—P exchange. Differences in DM exchange potential along the transect are likely impacted by a) the concentration gradient in DM between benthic and pelagic environments, b) variability in sediment grain size, c) active exchange processes through biological sediment reworking, d) the placement of solutes in the water column through anthropogenic disturbances (trawling), and e) the potential for shear stress-driven nutrient fluxes.

Sediments in the area were a net source of phosphate and silicic acid, potentially indicating a lack of uptake through benthic biological activity but a net sink for nitrogen, which is why no distinct efflux was detected here from the sediment into the water for any of the nitrogen compounds. Phosphate fluxes in particular are typically linked with organic carbon concentration in the sediment through iron oxide selectively binding either or both compounds, depending on oxygen availability (see Faust et al., 2020, 2021). Based on this study's results, the direction of DM flux is linked to ambient phosphate concentrations (pelagic and benthic), thereby also to the community composition of pelagic primary producers, which also depends on temperature (Downes et al., 2020). It should be noted, that the near-surface primary production is somewhat de-coupled from the planktonic and ice algal matter arriving on the seafloor through both space (lateral transport) and time (non-instantaneous sinking). Because of these delays, we cannot be certain that the community observed near the surface during sampling did in fact contribute to the benthic organic matter measured on the seabed. Nevertheless, there is a link between the two systems that must be considered, and Stevenson et al. (2023) found that the pigments measured on the sediment surface indicate recent depositions of ice algal and planktonic matter (based on data from the same cruises). The fact that phosphate concentrations were an important factor while silicic acid concentrations were not, even though both were considered equally, indicates the clarity of distinction in microbial phosphate uptake and processing in the water column between the southern and the northern regions, identified also by Downes et al. (2020) from samples taken on the same 2018 cruise. Atlantic influxes supply large amounts of phosphate to the Barents Sea from the South, which can be taken up and retained by the pelagic phytoplankton and microbial community (Downes et al., 2020). Locations dominated by Arctic water on the other hand, show overall lower ambient pelagic phosphate concentrations and

lower microbial uptake rates, but also an emission of organic phosphorous compounds by the microbial community (Downes et al., 2020). The planktonic community composition may respond to low pelagic phosphate concentrations in surface waters by shifting towards species that can modify their stoichiometric requirements to take up less phosphate in relation to other nutrients, or those that are capable of concentrating phosphate (e.g. Van Mooy et al., 2009). Depending on the bloom, the net downward fluxes recorded at the southern stations and net upward fluxes in the North may thus also correspond to the respective concentration gradients in phosphate between benthic and pelagic environments. Pelagic primary productivity supported or limited by these nutrient dynamics is in turn linked with vertical OM export, one of the main PM exchange processes.

A climate driven shift in the magnitude and dominant direction of passive phosphate B—P exchanges from upward to downward is possible, should northern conditions become more similar to those currently observed south of the Polar Front. DM flux activity at flow speeds below the critical erosion velocity, as observed at this location, implies that solutes within the pore water can cross the sediment-water boundary despite the cohesive nature of the sediment. This could be attributed to diffusive flow, in cases such as with the Ammonia fluxes that did not increase in line with the increased current speed. Solutes of which the concentration increases in the overlying water correlate closely with the increase in current velocity are more likely to be transported through advection. Biologically-mediated active DM exchange processes are dependent on macrofauna community composition and biodiversity, both of which have been found to vary between Atlantic and Arctic dominated benthic environments and are likely to be affected by climate change (Carroll and Ambrose Jr, 2012; Cochrane et al., 2012; Jørgensen et al., 2015). A northward shift of the Polar Front (Oziel et al., 2016) and increases in pelagic primary production in the northern parts of the Barents Sea (Lewis et al., 2020) are predicted to cause an increase in benthic biomass in the north (Cochrane et al., 2009). Based on our bioturbation estimates, this could thus increase bioturbation depths and surface boundary roughness in these areas if community structures remain comparable to those we observed, thereby raising the potential for biologically-driven B—P exchanges. However, climate driven changes in community assemblages may lead to different functional compositions of communities than we see at present, as climate change unfolds in the region, given that species response (to climate change) and effect (on sedimentary properties) traits do not necessarily correlate (Beauchard et al., 2017). Assuming that benthic community structure around the Polar Front would remain reflective of today's communities, as the front moves north, it would be unlikely that the heightened small-scale topographic diversity will cause a rise in advective fluxes, because the cohesive sediment matrix within Barents Sea glacial troughs does not promote this mechanism (Maiti et al., 2010; Rühl et al., 2020b). At the southern stations however, the northward shift of the Polar Front may benefit the pelagic environment, and cause changes in the benthos in areas which are currently covered by sea ice for part of the year (Søreide et al., 2013), through for example a reduction in organic matter input from ice algal sources to the benthos. This could lead to changes in benthic macrofaunal biomass and abundance as well as biogenically managed carbon storage potential (Boetius et al., 2013; Orlova et al., 2015; Faust et al., 2020). Increased availability of light and warmer water due to the absence of the sea ice promote phytoplanktonic production (Søreide et al., 2013) that also serve as an important food source to the benthos. Evidence shows that adaptation to the changed food type is likely possible (Mäkelä et al., 2017).

Another factor closely related to sea ice cover is trawling: Present-day observations indicate a contrast between high trawling efforts at the southern stations, which are either infrequently, or never covered by sea ice, with little to no trawling in the North, as indicated by AIS logs. Fishing fleets can be expected to exploit the increasingly available fishing grounds following the retreat of the ice and northward-shifting distribution of commercially-important boreal species (Fossheim et al., 2015; Misund et al., 2016; Fauchald et al., 2021). Estimated trawling efforts were identified here as one of the drivers of the current differences in DM B—P exchange direction and magnitude, and trawling intensity is a well-known key driver of change in benthic communities (Hiddink et al., 2006). The predicted re-distribution of trawling activity may thus cause changes to these communities and processes as well, though the magnitude of this cannot be assessed in the scope of this study.

Factors of statistical importance to the differences in PM B—P exchange between the southern, upward-dominated transport, and the northern, downward – dominated transport, Barents Sea, were measures of suspended matter, bioturbation and anthropogenic sediment disturbance. The discrepancy between estimated near bed and critical erosion velocities shows that naturally occurring velocities would not induce resuspension. Station B16 is the only possible exception, though sediment properties at this site do not indicate frequent resuspension or particle winnowing. The OPLS modelling of PM exchange drivers indicates that although physical anthropogenic disturbances play a significant role in modifying benthic-pelagic exchanges in this environment, they are of a similar importance as benthic biological activity, which also contributes significantly to PM B—P exchanges. The higher abundance at equal biomass at station B16, compared to the other stations, suggests smaller organisms, which indicates that the biologically driven benthic recycling processes are weaker at this location. However, as the observed variability in bioturbation depth and resulting surface boundary roughness was in dependence of ice cover levels rather than location, it's unlikely that the larger amount of smaller organisms at this station would lead to a difference in biogenic sediment transport. Changes in environmental circumstance have the potential to influence benthic macrofaunal trait expression, thereby affecting community behaviour and ecosystem functioning (Cassidy et al., 2020; Dolbeth et al., 2019). Solan et al. (2020) shows a clear link between trait composition and OM input and timing in the study area, both of which are projected to change under future conditions at this location.

Previous findings, that sedimentary particle mixing in glacial trough environments is predominantly biologically driven (Maiti et al., 2010), had not taken anthropogenic drivers into account. Considering that trawling is also known to impact on the structure of benthic macrofauna (Puig et al., 2012; Hiddink et al., 2006) and megafauna communities (Jørgensen et al., 2016) and suspended matter concentration (Palanques et al., 2001), this factor may be especially important in determining climate-driven changes in PM B—P exchange. One possible outcome could be, that a decrease in benthic biological activity could lead to higher rates of long-term OC burial due to lower biogenic carbon processing efficiency in the southern Barents Sea (Søreide et al., 2013; Stevenson and Abbott, 2019). At present, the Barents Sea is the largest sink of OC of all Arctic shelf seas, and carbon assimilation and sedimentation rates are higher in the north than in the south (Carroll et al., 2008b). Future conditions could thus potentially promote an altered carbon processing balance, limiting upward fluxes south of the Polar Front.

Under current conditions, ambient suspended OM levels in near-bottom water were highest at the southernmost station and in ice-free conditions, both SPM and suspended OM concentrations decreased with increasing latitude. This could mean that with the retreating sea ice

and northward shift in the Polar Front, SPM and OM concentrations in the North may increase, which would also enhance the potential for biogeochemical cycling. The significance of differences in ambient SPM and suspended OM between the southern and the northern areas may be seen as representative of the importance of the pelagic OM production.

By exploring the potential of climate change to alter PM B—P exchanges, this study incites a rethinking of current perceptions of Arctic B—P coupling. So far, most studies have focussed on the downward flux of organic matter produced in the pelagic and supplied to the benthic environment (e.g. Grebmeier et al., 1988; Grebmeier, 1993; Ambrose and Renaud, 1995; Dunton et al., 2005; Tamelander et al., 2006; Morata, 2007; Renaud et al., 2008; Søreide et al., 2013; Stasko et al., 2018). The current study integrates both downward and upward B—P exchange processes and includes not only their biological drivers, but also their biogeochemical, physical and anthropogenic ones. In addition, of the existing studies of climate change effects on B—P coupling in the Arctic, most tend to focus only on the consequences of reduced organic matter input due to sea ice loss (e.g. Thamdrup and Fleischer, 1998; Mattlin et al., 2000; Fortier et al., 2002; Marcin Węsławski et al., 2011; Birchenough et al., 2015). While this is also addressed here, the transdisciplinary approach facilitates the detection of other likely climate change impacts such as changes in magnitude and direction of B—P exchange processes. A small number of previous studies have explored climate change effects in the Arctic incorporating oceanographic and geophysical, as well as biological elements (Carroll and Carroll, 1990; Nishi and Tabeta, 2007; Søreide et al., 2013), but our study is the first to also consider the effects of a potential increase in anthropogenic pressures. Further studies on this matter are needed to better understand the magnitude of the issue and its potential impacts, including modelling efforts to quantify fluxes over larger spatial scales and predict future changes comprehensively.A limitation of the current study is that it captures only a snapshot of each of two years. Without the context of previous studies or long-term records for most of the variables (excluding sea ice cover (Cryo, 2019), trawling effort (Global Fishing Watch, 2020) and sediment grain size (Norges Geologiske Undersøkelse, 2020)), there is little indication of whether, or how much, the conditions recorded in this study have already been altered due to climate change effects. It is however clear that the current conditions are unlikely to be "unaltered", as the effects of climate change have been noted in the Barents Sea for over 50 years (Onarheim and Årthun, 2017), and trawling activity has been present in the area since the 1930s (Nordic Council of Ministers, 2007). Longer observational records, spanning multiple spring and neap tides, are also needed to ascertain how often an exceedance of critical erosion velocities could occur. It is uncertain whether such conditions, as observed at B16, are a common occurrence or an exceptional circumstance. Furthermore, the specific nature of conditions found within glacial trough areas limits how applicable the findings of this study are to the Barents Sea Shelf in general (see e.g. Cochrane et al., 2012) and the small number of sampling stations spread over the rather long transect lead to limited spatial data coverage. Further studies with a higher spatial data coverage would be extremely beneficial to better understand how representative the patterns observed here are. This is particularly true for bioirrigation, which was variable between stations south and north of the Polar Front and bioturbation, which in relation to ice cover, as both data sets were collected in 2017 and 2018 rather than 2018 and 2019 alongside the rest of the data. Using modelling approaches to determine fluxes on a larger and more representative scale would be a good way to mitigate the spatiotemporal limitations of the experimental approach used here. This was done in a different study resulting from the same project work, published by Freitas et al. (2020). Here, benthic-pelagic OM transport and nutrient fluxes were modelled in anticipation of climate-driven changes to the Arctic environment. Multi-annual observations would be beneficial in quantifying inter-annual variability of these, and other, parameters. The lack of ADCP data in 2018 introduces an element of uncertainty, which should be amended by undertaking further observations of the currents in the area in future studies. It should also be noted that the limitation of the ship-board CT-room temperatures to a minimum of 2 °C may have had an impact on the resuspension experiments, as in-situ temperatures were in some cases lower, at the northern stations in particular. Ideally, trawling data with lower uncertainty levels regarding gear type and fishing intensity would be available to provide an opportunity to detect potentially anthropogenically driven exchanges more definitively.

## 5. Conclusion

The exchange of particulate and dissolved matter in the Barents Sea, as well as many of the processes driving it, is likely to change as the Polar Front moves further north and the sea ice retreats due to climate change. Whereas under current conditions there is a net downward flux of particles and a net upward flux of solutes in the region north of the Polar Front, flux directions could be reversed and magnitudes of exchange altered drastically in the future. The work presented in this study should be used as a basis for future studies of the same processes in a more diverse selection of Arctic habitats, to allow conclusions about climate-driven changes to B—P exchange drivers and processes in the wider Barents Sea and overall Arctic area to be drawn. The data and ecosystem functions described above provide valuable information about the Barents Sea that can be used in the validation of ecosystem models of the area and form the basis for further research.

## CRediT authorship contribution statement

**Saskia Rühl:** Writing – original draft, Methodology, Investigation, Formal analysis, Data curation, Conceptualization. **Charlotte E.L. Thompson:** Writing – review & editing, Methodology, Funding acquisition, Conceptualization. **Ana M. Queirós:** Writing – review & editing, Methodology, Funding acquisition, Conceptualization. **Joanne E. Hopkins:** Writing – review & editing, Writing – original draft, Methodology, Formal analysis, Data curation. **Sian F. Henley:** Writing – review & editing, Writing – original draft, Methodology, Formal analysis, Data curation. **Stephen Widdicombe:** Writing – review & editing, Supervision, Methodology, Funding acquisition, Conceptualization.

## Declaration of competing interest

The authors declare the following financial interests/personal relationships which may be considered as potential competing interests:

Saskia Rühl reports financial support was provided by Natural Environment Research Council. Steve Widdicombe reports financial support was provided by Natural Environment Research Council. Steve Widdicombe reports financial support was provided by German Federal Ministry of Education and Research. Saskia Rühl reports financial support was provided by Estuarine & Coastal Sciences Association. If there are other authors, they declare that they have no known competing

financial interests or personal relationships that could have appeared to influence the work reported in this paper.

## Acknowledgements

This work was supported by "The Changing Arctic Ocean Seafloor (ChAOS)" [NE/N015894/1, NE/P006426/1, and NE/P006108/1, 2017-2021] and ARISE [NE/P006000/2] projects, which were both part of the Changing Arctic Ocean programme, jointly funded by the UKRI Natural Environment Research Council (NERC) and the German Federal Ministry of Education and Research (BMBF). Studentship funding [NE/L002531/1] was provided through the NERC. The Estuarine and Coastal Sciences Association is thanked for bestowing the Charles Boyden Award to partially fund a revised set of box corer boxes, which made sampling during the 2019 cruise vastly easier. Prof M. Solan, E.R. Ward, C.L. Wood, Dr. A.J. Reed, Dr. L.J. Grange and Dr. J.A. Godbold are thanked for making their bioturbation and bioirrigation data accessible for analysis in this publication. Dr. R. Airs and Dr. B. Zänker are thanked for providing information on benthic pigment and TEP. The authors would also like to thank Dr. L. Talbot, Prof M. Solan, J. Beja, Dr. R. Coppock, J. Nunes, E.R. Ward, Dr. J.A. Godbold, C. Walkinshaw, T. Mesher, E. Broad, C.L. Wood, N. Ensor, Dr. E. Venables, Dr. A.J. Reed and R. Owen for their help in collecting samples. We are also indebted to the crew and engineering team of the RSS James Clark Ross and the National Marine Facilities scientific engineers who provided technical assistance and advice throughout both cruises.

## Appendix A. Appendices

**Table A.1**
Exact locations of replicate box cores.

| Cruise | Station | Repetition | Latitude | Longitude | Depth in m |
|---|---|---|---|---|---|
| JR17007 | B13 | 1 | 74.49993 | 29.9996 | 358 |
| JR17007 | B13 | 2 | 74.49995 | 29.99891 | 358 |
| JR17007 | B13 | 3 | 74.49945 | 29.9983 | 367 |
| JR17007 | B13 | 4 | 74.49931 | 29.99792 | 367 |
| JR17007 | B13 | 5 | 74.49923 | 29.99841 | 364 |
| JR17007 | B14 | 1 | 76.49956 | 30.49896 | 292 |
| JR17007 | B14 | 2 | 76.49949 | 30.49837 | 292 |
| JR17007 | B14 | 3 | 76.49934 | 30.49808 | 292 |
| JR17007 | B14 | 4 | 76.49925 | 30.49869 | 293 |
| JR17007 | B14 | 5 | 76.49934 | 30.49927 | 293 |
| JR17007 | B15 | 1 | 78.52122 | 29.99896 | 312 |
| JR17007 | B15 | 2 | 78.25095 | 29.99772 | 311 |
| JR17007 | B15 | 3 | 78.25098 | 29.99917 | 311 |
| JR17007 | B15 | 4 | 78.25114 | 29.999 | 311 |
| JR17007 | B15 | 5 | 78.25123 | 29.99972 | 312 |
| JR17007 | B16 | 1 | 80.11607 | 30.06703 | 279 |
| JR17007 | B16 | 2 | 80.116 | 30.06609 | 278 |
| JR17007 | B16 | 3 | 80.11581 | 30.06556 | 283 |
| JR17007 | B16 | 4 | 80.11595 | 30.06635 | 283 |
| JR17007 | B16 | 5 | 80.11597 | 30.06514 | 284 |
| JR17007 | B17 | 1 | 81.28125 | 29.3254 | 334 |
| JR17007 | B17 | 2 | 81.28114 | 29.32433 | 334 |
| JR17007 | B17 | 3 | 81.28089 | 29.32487 | 334 |
| JR17007 | B17 | 4 | 81.281 | 29.32565 | 335 |
| JR17007 | B17 | 5 | 81.28107 | 29.32666 | 335 |
| JR18006 | B13 | 1 | 74.46575 | 30.11817 | 353.93 |
| JR18006 | B13 | 2 | 74.46589 | 30.11805 | 353.89 |
| JR18006 | B13 | 3 | 74.46596 | 30.11818 | 353.74 |
| JR18006 | B13 | 4 | 74.46602 | 30.11822 | 355.72 |
| JR18006 | B13 | 5 | 74.46609 | 30.11837 | 354.36 |
| JR18006 | B14 | 1 | 76.55236 | 30.61845 | 281.32 |
| JR18006 | B14 | 2 | 7,655,217 | 30.61811 | 281.53 |
| JR18006 | B14 | 3 | 76.552 | 30.61769 | 281.39 |
| JR18006 | B14 | 4 | 76.55183 | 30.6173 | 281.74 |
| JR18006 | B14 | 5 | 76.55177 | 30.61711 | 281.11 |
| JR18006 | B15 | 1 | 78.26153 | 30.20271 | 312 |
| JR18006 | B15 | 2 | 78.26137 | 30.20164 | 313 |
| JR18006 | B15 | 3 | 78.26126 | 30.20075 | 313 |
| JR18006 | B15 | 4 | 78.26125 | 30.20045 | 343 |
| JR18006 | B15 | 5 | 78.26117 | 30.19994 | 313 |
| JR18006 | B16 | 1 | 80.06242 | 29.92257 | 296 |
| JR18006 | B16 | 2 | 80.07458 | 29.92959 | 293 |
| JR18006 | B16 | 3 | 80.08279 | 29.93968 | 300 |
| JR18006 | B16 | 4 | 80.08899 | 29.95215 | 299 |
| JR18006 | B16 | 5 | 80.10068 | 29.98869 | 296 |

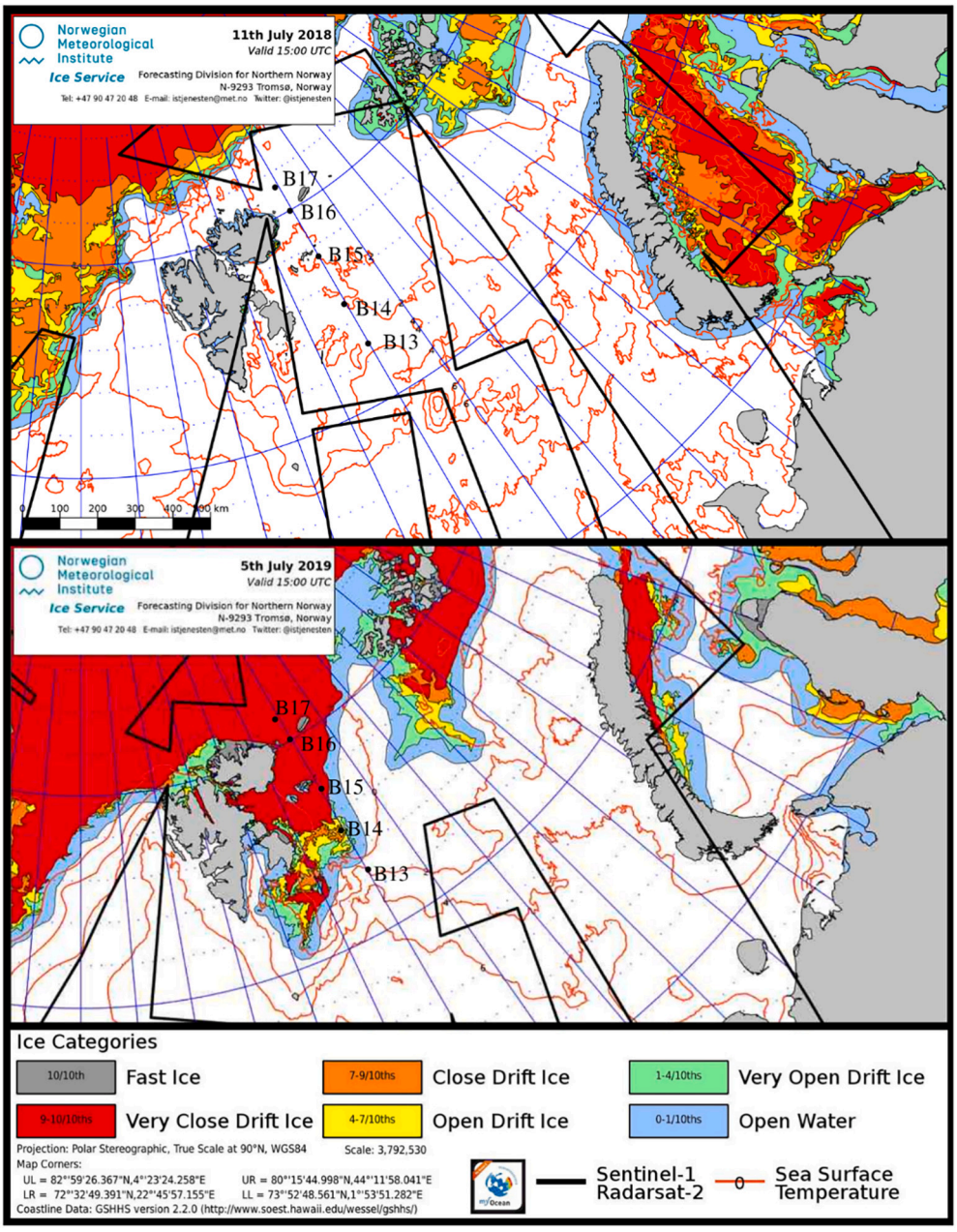


**Fig. B.1.** Sea Ice cover. Top: Sea ice cover immediately before the beginning of JR17007 cruise on 11th July 2018. Bottom: Sea ice cover immediately before the beginning of the JR18006 cruise on the 5th July 2019. Sea ice maps generated through the Norwegian Meteorological Institute Ice Service, (Cryo, 2019); approximate positions of stations B13-B17 are indicated by black markers on sea ice maps.

**Table C.1**
Locations and depths of the CTD bottom water samples and distances between replicate box cores in m.

| Cruise | Station | Latitude | Longitude | Depth in m | Average distance between reps in m |
|---|---|---|---|---|---|
| JR17007 | B13 | 74.3 | 30.0002 | 359 / 357 | 207.427 |
| JR17007 | B14 | 76.3 | 30.3001 | 292 | 25.424 |
| JR17007 | B15 | 78.1511 | 29.5995 | 313 | 28.599 |
| JR17007 | B16 | 80.07 | 30.0411 | 280 | 22.99 |
| JR17007 | B17 | 81.1689 | 29.1959 | 334 | 28.943 |
| JR18006 | B13 | 74.3 | 30.0002 | 359.1 | 18.712 |
| JR18006 | B14 | 76.3 | 30.3001 | 295.4 | 38.251 |
| JR18006 | B15 | 78.1511 | 29.5995 | 318.4 | 35.818 |
| JR18006 | B16 | 80.07 | 30.0412 | 288.4 | 2120.684 |

**Table D.1**
Times and dates during which sampling stations were visited.

| Cruise | Station | From | To |
|---|---|---|---|
| JR17007 | B13 | 14/07/2018 07:38 | 15/07/2018 12:27 |
| JR17007 | B14 | 25/07/2018 01:53 | 26/07/2018 01:26 |
| JR17007 | B15 | 16/07/2018 11:37 | 17/07/2018 10:37 |
| JR17007 | B16 | 22/07/2018 10:18 | 23/07/2018 19:01 |
| JR17007 | B17 | 18/07/2018 06:37 | 19/07/2018 19:33 |
| JR18006 | B13 | 07/07/2019 16:18 | 09/07/2019 16:40 |
| JR18006 | B14 | 12/07/2019 17:49 | 14/07/2019 10:14 |
| JR18006 | B15 | 10/07/2019 16:59 | 12/07/2019 03:13 |
| JR18006 | B16 | 16/07/2019 03:51 | 17/07/2019 09:25 |

**Table E.1**
In-situ bottom-temperatures measured via CTD versus CT room settings.

| Cruise | Station | Bottom temperature (°C) | CT room setting (°C) | CT room actual (°C) |
|---|---|---|---|---|
| JR17007 | B13 | 1.34 | 2 | 2 |
| JR17007 | B14 | 1.54 | 2 | 2 |
| JR17007 | B15 | −0.58 | 0 | 0 |
| JR17007 | B16 | 0.39 | 0 | 0 |
| JR17007 | B17 | 0.98 | 0 | 0 |
| JR18006 | B13 | 1.48 | 2 | 2 |
| JR18006 | B14 | 0.87 | 0 | 2.4 |
| JR18006 | B15 | −1.82 | 0 | 2 |
| JR18006 | B16 | −1.83 | 0 | 1.9 |

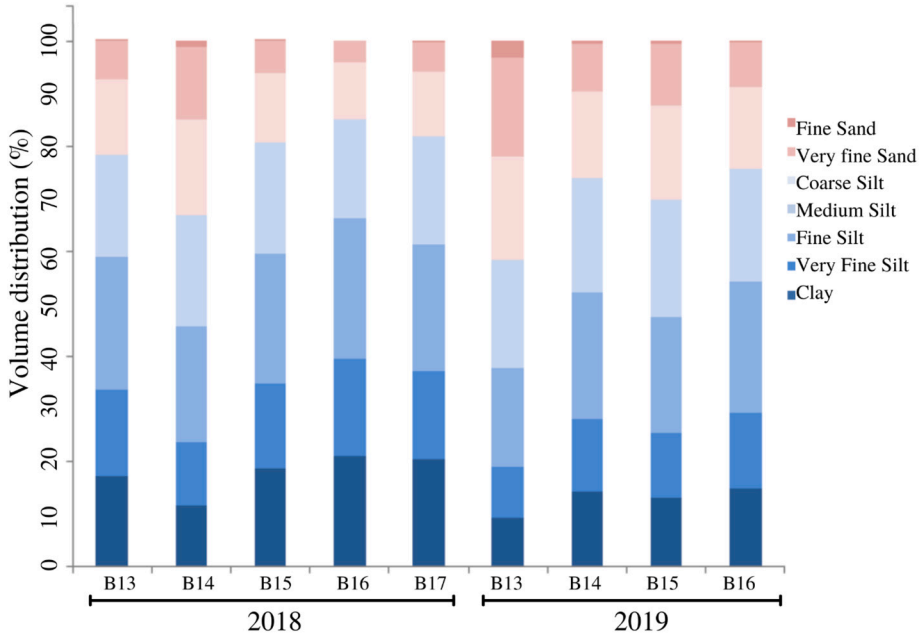


**Fig. F.1.** Sediment size fractions at each of the stations in 2018 and 2019.
SPM concentration across stress-driven resuspension cycle, starting roughly at the point of resuspension and increasing with rising applied shear stress. The points of various shapes represent data points of replicate samples and the lines represent averages of the replicates.

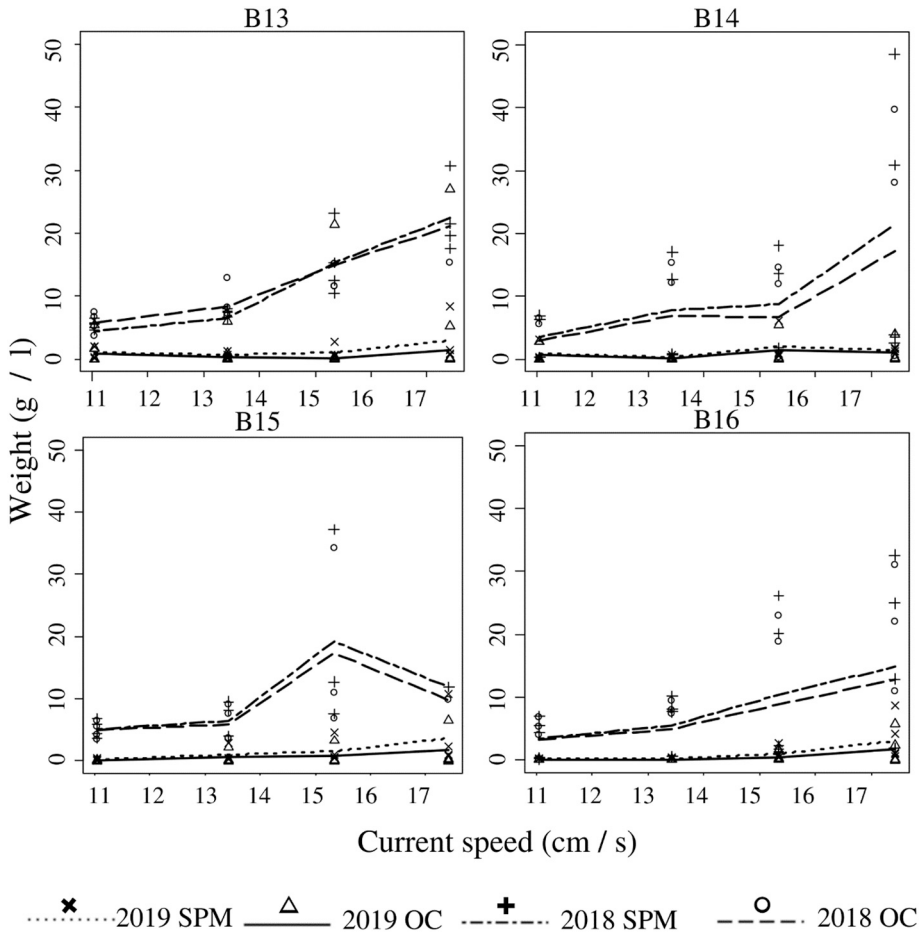


**Fig. G.1.** Barotropic tidal currents versus the depth average velocities. All data from 2019; (a-d) Predicted (dashed lines) east-west (blue) and north-south (red) velocities from the VMADCP (solid lines); (e-h) east-west versus north-south depth mean current measurements from the VMADCP at each site, the red dot in e-h indicates the mean.

**Table H.1**
OPLS models significant VIP scores.

| Model | Variable | VIP score |
|---|---|---|
| Model 1, DM all factors, stations as class | $d_{50}$ | 1.2783 |
| | Bioturbation depth | 1.5904 |
| | Surface boundary roughness | 1.2309 |
| | Biodiffusion coefficient | 1.7143 |
| | Annual trawling hours | 1.8260 |
| Model 2, DM all factors, north-south divide (B13–14 / B15–17) as class | $d_{50}$ | 1.2636 |
| | Pelagic phosphate concentration | 1.0398 |
| | Shear stress driven phosphate flux | 1.0160 |
| | Bioturbation depth | 1.1795 |
| | Biodiffusion coefficient | 1.6920 |
| | Annual trawling hours | 1.9417 |
| Model 3, PM all factors, stations as class | $d_{50}$ | 1.1546 |
| | Sediment TOM content | 1.3245 |
| | Ambient SPM concentration | 1.1551 |
| | Ambient suspended OM concentration | 1.2778 |
| | Bioturbation depth | 1.3669 |
| | Annual trawling hours | 1.6733 |
| Model 4, DM all factors, north-south divide (B13 / B14–17) as class | Ambient SPM concentration | 1.6059 |
| | Ambient suspended OM concentration | 1.6171 |
| | Bioturbation depth | 1.1862 |
| | Surface boundary roughness | 1.2424 |
| | Annual trawling hours | 1.6474 |

## Data availability

Data sets are available online, deposited via the BODC.

## References


Aagaard, K., Coachman, L.K., Carmack, E., 1981. On the halocline of the Arctic Ocean. Deep Sea Res. Part A 28 (6), 529–545. https://doi.org/10.1016/0198-0149(81)90115-1.

Ådlandsvik, B., Loeng, H., 1990. A study of the climatic system in the Barents Sea. Polar Res. 10 (1), 12–16. https://doi.org/10.3402/polar.v10i1.6726.

Ambrose, W.G., Renaud, P.E., 1995. Benthic response to water column productivity patterns: evidence for benthic-pelagic coupling in the Northeast Water Polynya. J. Geophys. Res. Oceans 100 (C3), 4411–4421. https://doi.org/10.1029/94JC01982@10.1002/(ISSN)2169-9291.LEADPOLY1.

Årthund, M., Eldevik, T., Smedsrud, L.H., Skagseth, Ø., Ingvaldsen, R.B., 2020. Quantifying the influence of Atlantic heat on Barents Sea ice variability and retreat. J. Clim. 25, 4736–4743. https://doi.org/10.1175/JCLI-D-11-00466.1.

Aschan, M.M., Trannum, H.C., 2006. Community Structure and Species Biodiversity in Benthic Fauna in the Deeper Barents Sea.

Barnes, D., Andrade, L., Braun, J., Broad, E., Brunner, L., Downes, P., et al., 2019. Changing Arctic Ocean Seafloor JR18006 Cruise Report (Issue August).

Barton, B.I., Lenn, Y.D., Lique, C., 2018. Observed atlantification of the Barents Sea causes the Polar Front to limit the expansion of winter sea ice. J. Phys. Oceanogr. 48 (8), 1849–1866. https://doi.org/10.1175/JPO-D-18-0003.1.

Beauchard, O., Veríssimo, H., Queirós, A.M., Herman, P.M.J., 2017. The use of multiple biological traits in marine community ecology and its potential in ecological indicator development. Ecol. Indic. 76, 81–96. https://doi.org/10.1016/j.ecolind.2017.01.011.

Birchenough, S.N.R., Reiss, H., Degraer, S., Mieszkowska, N., Borja, Á., Buhl-Mortensen, L., et al., 2015. Climate change and marine benthos: a review of existing research and future directions in the North Atlantic. Wiley Interdiscip. Rev. Clim. Chang. 6 (2), 203–223. https://doi.org/10.1002/wcc.330.

Boetius, A., Albrecht, S., Bakker, K., Bienhold, C., Felden, J., Fernández-Méndez, M., Hendricks, S., Katlein, C., Lalande, C., Krumpen, T., Nicolaus, M., 2013. Export of algal biomass from the melting Arctic sea ice. Science 339 (6126), 1430–1432. https://doi.org/10.1126/science.1231346.

Breusch, T.S., Pagan, A.R., 1979. A simple test for heteroskedasticity and coefficient variation. Econometrica 47 (5), 1287–1294.

Bylesjö, M., Rantalainen, M., Cloarec, O., Nicholson, J.K., Holmes, E., Trygg, J., 2006. OPLS discriminant analysis: combining the strengths of PLS-DA and SIMCA classification. J. Chemom. 20, 341–351. https://doi.org/10.1002/cem.

Carroll, M.L., Ambrose Jr., W.G., 2012. Benthic infaunal community variability on the northern Svalbard shelf. Polar Biol. 35, 1259–1272. https://doi.org/10.1007/s00300-012-1171-x.

Carroll, M., Carroll, J., 1990. The Arctic seas. In: Black, K.D., Shimmield, G.B. (Eds.), Biogeochemistry of Marine Systems. Blackwell Publishing Ltd.

Carroll, M.L., Denisenko, S.G., Renaud, P.E., Ambrose, W.G., 2008a. Benthic infauna of the seasonally ice-covered western Barents Sea: patterns and relationships to environmental forcing. Deep-Sea Res. Part II 55 (20−21), 2340–2351. https://doi.org/10.1016/j.dsr2.2008.05.022.

Carroll, J.L., Zaborska, A., Papucci, C., Schirone, A., Carroll, M.L., Pempkowiak, J., 2008b. Accumulation of organic carbon in western Barents Sea sediments. Deep-Sea Res. Part II 55 (20–21), 2361–2371. https://doi.org/10.1016/j.dsr2.2008.05.005.

Cassidy, C., Grange, L.J., Garcia, C., Bolam, S.G., Godbold, J.A., 2020. Species interactions and environmental context affect intraspecific behavioural trait variation and ecosystem function. Proc. R. Soc. Biol. 287, 1–10. https://doi.org/10.1098/rspb.2019.2143.

Cochrane, S.K.J., Denisenko, S.G., Renaud, P.E., Emblow, C.S., Ambrose, W.G., Ellingsen, I.H., et al., 2009. Benthic macrofauna and productivity regimes in the Barents Sea-ecological implications in a changing Arctic. J. Sea Res. 61, 222–233. https://doi.org/10.1016/j.seares.2009.01.003.

Cochrane, S.K.J., Pearson, T.H., Greenacre, M., Costelloe, J., Ellingsen, I.H., Dahle, S., et al., 2012. Benthic fauna and functional traits along a Polar Front transect in the Barents Sea-Advancing tools for ecosystem-scale assessments. J. Mar. Syst. 94, 204–217. https://doi.org/10.1016/j.jmarsys.2011.12.001.

Coulter International Corporation, 1996. Coulter LS Series. http://www.cyto.purdue.edu/cdroms/cyto2/6/coulter/ss000096.htm.

Cryo.met.no [Internet]. Norwegian Meteorological Institute Ice Service. Operational Ice Charts. [cited 2019]. Available from: https://cryo.met.no/.

Denisenko, S.G., Denisenko, N.V., Lehtonen, K.K., Andersin, A.B., Laine, A.O., 2003. Macrozoobenthos of the Pechora Sea (SE Barents Sea): community structure and spatial distribution in relation to environmental conditions. Mar. Ecol. Prog. Ser. 258, 109–123. https://doi.org/10.3354/meps258109.

Dolbeth, M., Crespo, D., Leston, S., Solan, M., 2019. Realistic scenarios of environmental disturbance lead to functionally important changes in benthic species-environment interactions. Mar. Environ. Res. 150 (May), 104770. https://doi.org/10.1016/j.marenvres.2019.104770.

Downes, P., Goult, S., Woodward, M., Widdicombe, C., Tait, K., Dixon, J., 2020. Phosphorus dynamics in the Barents Sea. Limnol. Oceanogr. 66 (51), 326–342.

Dunton, K.H., Goodall, J.L., Schonberg, S.V., Grebmeier, J.M., Maidment, D.R., 2005. Multi-decadal synthesis of benthic-pelagic coupling in the western arctic: role of cross-shelf advective processes. Deep-Sea Res. Part II 52 (24–26), 3462–3477. https://doi.org/10.1016/j.dsr2.2005.09.007.

Egbert, G.D., Erofeeva, S.Y., 2002. Efficient inverse modeling of barotropic ocean tides. J. Atmos. Ocean. Technol. 19, 183–204.

Egea, L.G., Infantes, E., Jiménez-Ramos, R., 2023. Loss of POC and DOC on seagrass sediments by hydrodynamics. Sci. Total Environ. 901, 165976. https://doi.org/10.1016/j.scitotenv.2023.165976.

Ellingsen, I.H., Dalpadado, P., Slagstad, D., Loeng, H., 2007. Impact of climatic change on the biological production in the Barents Sea. Clim. Chang. 87, 155–175. https://doi.org/10.1007/s10584-007-9369-6.

Faleide, J.I., Solheim, A., Fiedler, A., Hjelstuen, B.O., Andersen, E.S., Vanneste, K., 1996. Late Cenozoic evolution of the western Barents Sea-Svalbard continental margin. Glob. Planet. Chang. 12 (1–4), 53–74. https://doi.org/10.1016/0921-8181(95)00012-7.

Fauchald, P., Arneberg, P., Debernard, J.B., Lind, S., Olsen, E., Hausner, V.H., 2021. Poleward shifts in marine fisheries under Arctic warming. Environ. Res. Lett. 16 (7), 074057. https://doi.org/10.1088/1748-9326/ac1010.

Faust, J.C., Stevenson, M.A., Abbott, G.D., Knies, J., Tessin, A., Mannion, I., Ford, A., Hilton, R.G., Peakall, J., März, C., 2020. Does Arctic warming reduce preservation of organic matter in Barents Sea sediments? Phil. Trans. R. Soc. A 378, 20190364. https://doi.org/10.1098/rsta.2019.0364.

Faust, J.C., Tessin, A., Fisher, B.J., Zindorf, M., Papadaki, S., Hendry, K.R., Doyle, K.A., März, C., 2021. Millennial scale persistence of organic carbon bound to iron in Arctic marine sediments. Nat. Commun. 12 (1), 275. https://doi.org/10.1038/s41467-020-20550-0.

Ferrari, R., Jansen, M.F., Adkins, J.F., Burke, A., Stewart, A.L., Thompson, A.F., et al., 2014. Antarctic sea ice control on ocean circulation in present and glacial climates. PNAS 111 (24), 8753–8758. https://doi.org/10.1073/pnas.1323922111.

Fortier, M., Fortier, L., Michel, C., Legendre, L., 2002. Climatic and biological forcing of the vertical flux of biogenic particles under seasonal Arctic sea ice. Mar. Ecol. Prog. Ser. 225, 1–16. https://doi.org/10.3354/meps225001.

Fossheim, M., Nilssen, E.M., Aschan, M., 2006. Fish assemblages in the Barents Sea. Mar. Biol. Res. 2 (4), 260–269. https://doi.org/10.1080/17451000600815698.

Fossheim, M., Primicerio, R., Johannesen, E., Ingvaldsen, R.B., Aschan, M.M., Dolgov, A. V., 2015. Recent warming leads to a rapid borealization of fish communities in the Arctic. Nat. Clim. Chang. 5 (7), 673–677. https://doi.org/10.1038/nclimate2647.

Freitas, F.S., Hendry, K.R., Henley, S.F., Faust, J.C., Tessin, A.C., Stevenson, M.A., Abbott, G.D., März, C., Arndt, S., 2020. Benthic-pelagic coupling in the Barents Sea: An integrated data-model framework. Philos. Trans. R. Soc. A 378 (2181), 20190359.

Furevik, T., Drange, H., Sorteberg, A., 2002. Anticipated changes in the Nordic seas marine climate. Fisken Og Havet 4, 1–13. http://zubov.atmos.uiuc.edu/ACIA/.

Fyfe, J.C., Boer, G.J., Flato, G.M., 1999. The Arctic and Antarctic oscillations and their projected changes under global warming. Geophys. Res. Lett. 26 (11), 1601–1604. https://doi.org/10.1029/1999GL900317.

Giraud, X., Le Quéré, C., da Cunha, L.C., 2008. Importance of coastal nutrient supply for global ocean biogeochemistry. Glob. Biogeochem. Cycles 22 (2), 1–15. https://doi.org/10.1029/2006GB002717.

Gjevik, B., Nøst, E., Straume, T., 1994. Model simulations of the tides in the Barents Sea. J. Geophys. Res. 99 (C2), 3337. https://doi.org/10.1029/93JC02743.

GlobalFishingWatch.org [Internet], 2020. Datasets and code. In: Anonymised AIS Data and Other Data cited. Available Online. https://globalfishingwatch.org/datasets-and-code/.

Grebmeier, J.M., 1993. Studies of pelagic-benthic coupling extended onto the Soviet continental shelf in the northern Bering and Chukchi seas. Cont. Shelf Res. 13 (5–6), 653–668. https://doi.org/10.1016/0278-4343(93)90098-I.

Grebmeier, J.M., Barry, J.P., 1991. The influence of oceanographic processes on pelagic-benthic coupling in polar regions: a benthic perspective. J. Mar. Syst. 2 (3–4), 495–518. https://doi.org/10.1016/0924-7963(91)90049-Z.

Grebmeier, J., McRoy, C., Feder, H., 1988. Pelagic-benthic coupling on the shelf of the northern Bering and Chukchi Seas. I. Food supply source and benthic bio-mass. Mar. Ecol. Prog. Ser. 48, 57–67. https://doi.org/10.3354/meps048057.

Griffiths, J.R., Kadin, M., Nascimento, F.J.A., Tamelander, T., Toernroos, A., Bonaglia, S., et al., 2017. The importance of benthic – pelagic coupling for marine ecosystem functioning in a changing world. Glob. Chang. Biol. 23, 2179–2196. https://doi.org/10.1111/gcb.13642.

Hach, US, Lachat Quikchem Flow Injection Analysis System [cited 2020]. Available Online. https://www.hach.com/flow-injection-analysis-fia/lachat-quikchem-flow-injection-analysis-system/family?productCategoryId=35547627752.

Hiddink, J.G., Jennings, S., Kaiser, M.J., Queirós, A.M., Duplisea, D.E., et al., 2006. Cumulative impacts of seabed trawl disturbance on benthic biomass, production, and species richness in different habitats. Can. J. Fish. Aquat. Sci. 736, 721–736. https://doi.org/10.1139/F05-266.

Hopkins, J., Norman, L., de la Vega, C., Kellock, C., Maerz, C., Tessin, A., et al., 2018. RRS James Clark Ross JR16006, 30 June-8 Aug 2017. The Changing Arctic Ocean Cruise JR16006, vol. 51.

ICES.dk [Internet], 2020. Catch statistics. In: Dataset Collections [cited. Available online. https://www.ices.dk/marine-data/dataset-collections/Pages/Fish-catch-and-stock-assessment.aspx.

Ingvaldsen, R.B., 2005. Width of the North Cape Current and location of the Polar Front in the western Barents Sea. Geophys. Res. Lett. 32 (16), L16603. https://doi.org/10.1029/2005GL023440.

Ingvaldsen, R.B., Asplin, L., Loeng, H., 2004. The seasonal cycle in the Atlantic transport to the Barents Sea during the years 1997-2001. Cont. Shelf Res. 24 (9), 1015–1032. https://doi.org/10.1016/j.csr.2004.02.011.

IPCC, 2019. IPCC Special Report on the Ocean and Cryosphere in a Changing Climate-Summary for Policymakers. Hamish Pritchard.

Ivshin, V.A., Trofimov, A.G., Titov, O.V., 2019. Barents Sea thermal frontal zones in 1960–2017: variability, weakening, shifting. ICES J. Mar. Sci. 76 (1), i3–i9. https://doi.org/10.1093/icesjms/fsz159.
Jørgensen, L.L., Ljubin, P., Skjoldal, H.R., Ingvaldsen, R.B., Anisimova, N., Manushin, I., 2015. Distribution of benthic megafauna in the Barents Sea: baseline for an ecosystem approach to management. ICES J. Mar. Sci. 72 (2), 595–613.
Jørgensen, L.L., Primicerio, R., Ingvaldsen, R.B., Fossheim, M., Strelkova, N., Thangstad, T.H., Manushin, I., Zakharov, D., 2019. Impact of multiple stressors on sea bed fauna in a warming Arctic. Mar. Ecol. Prog. Ser. 608, 1–12. https://doi.org/10.3354/meps12803.
Jørgensen, L.L., Planque, B., Thangstad, T.H., Certain, G., 2016. Vulnerability of megabenthic species to trawling in the Barents Sea. ICES J. Mar. Sci. 73 (Suppl_1), i84–i97.
Kowalik, Z., Proshutinsky, A.Y., 1994. The Arctic Ocean Tides. Geophys. Monogr. 85, 137–158. https://doi.org/10.1029/gm085p0137.
Kowalik, Z., Proshutinsky, A.Y., 1995. Topographic enhancement of tidal motion in the western Barents Sea. J. Geophys. Res. 100 (C2), 2613–2637. https://doi.org/10.1029/94JC02838.
Le Fouest, V., Postlethwaite, C., Morales Maqueda, M.A., Bélanger, S., Babin, M., 2011. On the role of tides and strong wind events in promoting summer primary production in the Barents Sea. Cont. Shelf Res. 31 (17), 1869–1879. https://doi.org/10.1016/j.csr.2011.08.013.
Lewis, K.M., Van Dijken, G.L., Arrigo, K.R., 2020. Changes in phytoplankton concentration now drive increased Arctic Ocean primary production. Science 369 (6500), 198–202. https://doi.org/10.1126/science.aay8380.
Lind, S., Ingvaldsen, R.B., Furevik, T., 2018. Arctic warming hotspot in the northern Barents Sea linked to declining sea-ice import. Nat. Clim. Chang. 8 (7), 634–639. https://doi.org/10.1038/s41558-018-0205-y.
Loeng, H., 1991. Features of the physical oceanographic conditions of the Barents Sea. Polar Res. 10 (1), 5–18. https://doi.org/10.1111/j.1751-8369.1991.tb00630.x.
Loeng, H., Ozhigin, V., Ådlandsvik, B., 1997. Water fluxes through the Barents Sea. ICES J. Mar. Sci. 54 (3), 310–317. https://doi.org/10.1006/jmsc.1996.0165.
Maiti, K., Carroll, J.L., Benitez-Nelson, C.R., 2010. Sedimentation and particle dynamics in the seasonal ice zone of the Barents Sea. J. Mar. Syst. 79 (1–2), 185–198. https://doi.org/10.1016/j.jmarsys.2009.09.001.
Mäkelä, A., Witte, U., Archambault, P., 2017. Ice algae versus phytoplankton: resource utilization by Arctic deep sea macroinfauna revealed through isotope labelling experiments. Mar. Ecol. Prog. Ser. 572, 1–18. https://doi.org/10.3354/meps12157.
Marcin Węsławski, J., Kendall, M.A., Włodarska-Kowalczuk, M., Iken, K., Kędra, M., Legezynska, J., et al., 2011. Climate change effects on Arctic fjord and coastal macrobenthic diversity-observations and predictions. Mar. Biodivers. 41, 71–85. https://doi.org/10.1007/s12526-010-0073-9.
Mattlin, R.H., Reynolds, J.E., Huntington, H.P., Pungowiyi, C., 2000. Impact of Changes in Sea Ice and Other Environmental Parameters in the Arctic.
McMahon, K.W., Hamady, L.L., Thorrold, S.R., 2013. Ocean ecogeochemistry: A review. Oceanogr. Mar. Biol. Annu. Rev. 51, 327–374.
Mehmood, T., Liland, K.H., Snipen, L., Saebø, S., 2012. A review of variable selection methods in Partial Least Squares Regression. Chemom. Intell. Lab. Syst. 118, 62–69. https://doi.org/10.1016/j.chemolab.2012.07.010.
Misund, O.A., Heggland, K., Skogseth, R., Falck, E., Gjøsæter, H., Sundet, J., et al., 2016. Norwegian fisheries in the Svalbard zone since 1980. Regulations, profitability and warming waters affect landings. Polar Sci. 10 (3), 312–322. https://doi.org/10.1016/j.polar.2016.02.001.
Morata, N., 2007. Sedimentary Pigments as Biomarkers of Spatial and Seasonal Variations in Arctic Pelagic-Benthic Coupling [University of Conneticut]. https://doi.org/10.1017/CBO9781107415324.004.
MOSJ [Internet], 2020. Sea Ice Extent in the Barents Sea and Fram Strait. cited. Available online. http://www.mosj.no/en/climate/ocean/sea-ice-extent-barents-sea-fram-strait.html.
Nishi, Y., Tabeta, S., 2007. Sunlight and tidal interaction as a mechanism of carbon transport in an ice-covered region: results of a coupled ice-ocean ecosystem model. Cont. Shelf Res. 27 (1), 1–19. https://doi.org/10.1016/j.csr.2006.08.005.
Nordic Council of Ministers, 2007. Bottom Trawling and Scallop Dredging in the Arctic: Impacts of Fishing on Non-target Species, Vulnerable Habitats and Cultural Heritage. TemaNord.
Norges Geologiske Undersøkelse [Internet], 2020. Norwegian Geological Survey. Ministry of Trade and Industry Norway cited. Available online. https://www.ngu.no/.
Norwegian Meteorological Institute [Internet], 2020. Cryo. Sea Ice Data. cited. Available online: https://cryo.met.no/en.
Oksanen, J., Blanchet, F.G., Friendly, M., Kindt, R., Legendre, P., Mcglinn, D., et al., 2019. Package "vegan.".
Olli, K., Wexels Riser, C., Wassmann, P., Ratkova, T., Arashkevich, E., Pasternak, A., 2002. Seasonal variation in vertical flux of biogenic matter in the marginal ice zone and the Central Barents Sea. J. Mar. Syst. 38 (1–2), 189–204. https://doi.org/10.1016/S0924-7963(02)00177-X.
Onarheim, I.H., Årthun, M., 2017. Toward an ice-free Barents Sea. Geophys. Res. Lett. 44 (16), 8387–8395. https://doi.org/10.1002/2017GL074304.
Onarheim, I.H., Eldevik, T., Smedsrud, L.H., Stroeve, J.C., 2018. Seasonal and regional manifestation of Arctic sea ice loss. J. Clim. 31 (12), 4917–4932. https://doi.org/10.1175/JCLI-D-17-0427.1.
Orlova, E.L., Dolgov, A.V., Renaud, P.E., Greenacre, M., Halsband, C., Ivshin, V.A., 2015. Climatic and ecological drivers of euphausiid community structure vary spatially in the Barents Sea: relationships from a long time series (1952–2009). Front. Mar. Sci. 1, 74. https://doi.org/10.3389/fmars.2014.00074. Jan 6.
Oziel, L., Sirven, J., Gascard, J.-C., 2016. The Barents Sea frontal zones and water masses variability (1980–2011). Ocean Sci. 12 (1), 169–184. https://doi.org/10.5194/os-12-169-2016.
Oziel, L., Baudena, A., Ardyna, M., Massicotte, P., Randelhoff, A., Sallée, J.-B., et al., 2020. Faster Atlantic currents drive poleward expansion of temperate phytoplankton in the Arctic Ocean. Nat. Commun. 11 (1705), 1–8. https://doi.org/10.1038/s41467-020-15485-5.
Padman, L., Erofeeva, S., 2004. A barotropic inverse tidal model for the Arctic Ocean. Geophys. Res. Lett. 31 (2). https://doi.org/10.1029/2003GL019003.
Palanques, A., Guillén, J., Puig, P., 2001. Impact of bottom trawling on water turbidity and muddy sediment of an unfished continental shelf. Limnol. Oceanogr. 46 (5), 1100–1110. https://doi.org/10.4319/lo.2001.46.5.1100.
Pearson, K., 1895. VII. Note on regression and inheritance in the case of two parents. Proc. R. Soc. Lond. 58, 347–352.
Pfirman, S.L., Bauch, D., Gammelsrød, T., 1994. The Northern Barents Sea: water mass distribution and modification. Geophys. Monogr. Ser. 85, 77–94.
Puig, P., Canals, M., Company, J.B., Martín, J., Amblas, D., Lastras, G., et al., 2012. Ploughing the deep sea floor. Nature 489 (7415), 286–289.
Queirós, A.M., Birchenough, S.N., Bremner, J., Godbold, J.A., Parker, R.E., Romero-Ramirez, A., Reiss, H., Solan, M., Somerfield, P.J., Van Colen, Van Hoey, G., 2013. A bioturbation classification of E uropean marine infaunal invertebrates. Ecol. Evol. 3 (11), 3958–3985.
Reigstad, M., Wassmann, P., Wexels Riser, C., Øygarden, S., Rey, F., 2002. Variations in hydrography, nutrients and chlorophyll a in the marginal ice-zone and the Central Barents Sea. J. Mar. Syst. 38, 9–29. https://doi.org/10.1016/S0924-7963(02)00167-7.
Renaud, P.E., Riedel, A., Michel, C., Morata, N., Gosselin, M., Juul-Pedersen, T., et al., 2007. Seasonal variation in benthic community oxygen demand: a response to an ice algal bloom in the Beaufort Sea, Canadian Arctic? J. Mar. Syst. 67, 1–12. https://doi.org/10.1016/j.jmarsys.2006.07.006.
Renaud, P.E., Morata, M., Carroll, M.L., Denisenko, S.G., Reigstad, M., 2008. Pelagic-benthic coupling in the western Barents Sea: processes and time scales. Deep-Sea Res. Part II 55 (20–21), 2340–2351. https://doi.org/10.1016/j.dsr2.2008.05.022.
Richards, K.J., 1990. Physical processes in the benthic boundary layer. Philos. Trans. R. Soc. Lond. A 331, 3–13.
Riebesell, U., Schloss, I., Smetacek, V., 1991. Aggregation of algae released from melting sea ice: implications for seeding and sedimentation. Polar Biol. 11, 239–248. https://doi.org/10.1007/BF00238457.
Rigor, I.G., Wallace, J.M., Colony, R.L., 2002. Response of Sea Ice to the Arctic Oscillation. J. Clim. 15, 2648–2663. http://iapb.apl.washington.edu.
Rippeth, T.P., Vlasenko, V., Stashchuk, N., Scannell, B.D., Green, J.A.M., Lincoln, B.J., et al., 2017. Tidal conversion and mixing poleward of the critical latitude (an Arctic case study). Geophys. Res. Lett. 44, 12349–12357. https://doi.org/10.1002/2017GL075310.
Rühl, S., Thompson, C., Queirós, A.M., Widdicombe, S., 2020a. Intra-annual patterns of benthic / pelagic fluxes of dissolved and particulate matter. Front. Mar. Sci. 7 (567193), 1–25. https://doi.org/10.3389/fmars.2020.567193.
Rühl, S., Thompson, C., Queirós, A.M., Widdicombe, S., 2020b. Missing links in the study of solute and particle exchange between the sea floor and water column. ICES J. Mar. Sci. 77 (5), 14–27.
Sakshaug, E., 1997. Biomass and productivity distributions and their variability in the Barents Sea. ICES J. Mar. Sci. 54, 341–350.
Schauer, U., Loeng, H., Rudels, B., Ozhigin, V.K., Dieck, W., 2002. Atlantic water flow through the Barents and Kara seas. Deep-Sea Res. I 49, 2281–2298.
Serreze, M.C., Barry, R.G., 2011. Processes and impacts of Arctic amplification: a research synthesis. Glob. Planet. Chang. 77 (1–2), 85–96. https://doi.org/10.1016/j.gloplacha.2011.03.004.
Solan, M., 2018. The Changing Arctic Ocean: Cruise Report RSS James Clarke Ross JR17007 (Issue August).
Solan, M., Ward, E.R., Wood, C.L., Reed, A.J., Grange, L.J., Godbold, J.A., 2020. Climate-driven benthic invertebrate activity and biogeochemical functioning across the Barents Sea polar front: climate driven benthic activity. Philos. Trans. R. Soc. A Math. Phys. Eng. Sci. 378 (2181). https://doi.org/10.1098/rsta.2019.0365.
Søreide, J.E., Carroll, M.L., Hop, H., Ambrose, W.G., Hegseth, E.N., Falk-Petersen, S., 2013. Sympagic-pelagic-benthic coupling in Arctic and Atlantic waters around Svalbard revealed by stable isotopic and fatty acid tracers. Mar. Biol. Res. 9 (9), 831–850. https://doi.org/10.1080/17451000.2013.775457.
Soulsby, R., 1997. Dynamics of marine sands: A manual for practical applications. In: Dynamics of Marine Sands: A Manual for Practical Applications. Thomas Telford Publications.
Souster, T.A., Barnes, D.K.A., Hopkins, J., 2020. Variation in zoobenthic blue carbon in the Arctic's Barents Sea shelf sediments. Phil. Trans. R. Soc. A 378, 1–18. https://doi.org/10.1098/rsta.2019.0362.
Spearman, C., 1904. The proof and measurement of association between two things. Am. J. Psychol. 15 (1), 72–101.
Sswat, M., Gulliksen, B., Menn, I., Sweetman, A.K., Piepenburg, D., 2015. Distribution and composition of the epibenthic megafauna north of Svalbard (Arctic). Polar Biol. 38, 861–877. https://doi.org/10.1007/s00300-015-1645-8.
Stasko, A., Bluhm, B., Michel, C., Archambault, P., Majewski, A., Reist, J., et al., 2018. Benthic-pelagic trophic coupling in an Arctic marine food web along vertical water mass and organic matter gradients. Mar. Ecol. Prog. Ser. 594, 1–19. https://doi.org/10.3354/meps12582.
Stevenson, M.A., Abbott, G.D., 2019. Exploring the composition of macromolecular organic matter in Arctic Ocean sediments under a changing sea ice gradient. J. Anal. Appl. Pyrolysis 140, 102–111. https://doi.org/10.1016/j.jaap.2019.02.006.

Stevenson, M.A., Airs, R.L., Abbott, G.D., 2023. Unprecedented sea-ice minima enhances algal production deposited at the Arctic seafloor. Environ. Res. Lett. 18 (11), 114046. https://doi.org/10.1088/1748-9326/ad044a.

Sundfjord, A., Fer, I., Kasajima, Y., Svendsen, H., 2007. Observations of turbulent mixing and hydrography in the marginal ice zone of the Barents Sea. J. Geophys. Res. 112 (C5), 1–23. https://doi.org/10.1029/2006JC003524.

Tamelander, T., Renaud, P.E., Hop, H., Carroll, M.L., Ambrose, W.G., Hobson, K.A., 2006. Trophic relationships and pelagic-benthic coupling during summer in the Barents Sea Marginal Ice Zone, revealed by stable carbon and nitrogen isotope measurements. Mar. Ecol. Prog. Ser. 310, 33–46. https://doi.org/10.3354/meps310033.

Thamdrup, B., Fleischer, S., 1998. Temperature dependence of oxygen respiration, nitrogen mineralization, and nitrification in Arctic sediments. Aquat. Microb. Ecol. 15, 191–199.

Thévenot, E.A., Roux, A., Xu, Y., Ezan, E., Junot, C., 2015. Analysis of the human adult urinary metabolome variations with age, body mass index, and gender by implementing a comprehensive workflow for univariate and OPLS statistical analyses. Article J. Proteome Res. 1–15. https://doi.org/10.1021/acs.jproteome.5b00354.

Thompson, C.E.L., Couceiro, F., Fones, G.R., Amos, C.L., 2013. Shipboard measurements of sediment stability using a small annular flume—Core Mini Flume (CMF). Limnol. Oceanogr. Methods 11, 604–615. https://doi.org/10.4319/lom.2013.11.604.

Thorsnes, T., Brunstad, H., Lå Gstad, P., Chand, S., 2016. Trawl marks, iceberg ploughmarks and possible whale-feeding marks, Barents Sea. In: Atlas of Submarine Glacial Landforms: Modern, Quaternary and Ancient. Geological Society, pp. 293–294. https://doi.org/10.1144/M46.101.

Ubertini, M., Lefebvre, S., Gangnery, A., Grangere, K., Le Gendre, R., Orvain, F., 2012. Spatial variability of benthic-pelagic coupling in an estuary ecosystem: consequences for microphytobenthos resuspension phenomenon. PLoS One. https://doi.org/10.1371/journal.pone.0044155.

Van Mooy, B.A.S., Fredricks, H.F., Pedler, B.E., Dyhrman, S.T., Karl, D.M., Koblížek, M., et al., 2009. Phytoplankton in the ocean use non-phosphorus lipids in response to phosphorus scarcity. Nat. Lett. 458 (7234), 69–72. https://doi.org/10.1038/nature07659.

Vorren, T.O., Lebesbye, E., Andreassen, K., Larsen, K.B., 1989. Glacigenic sediments on a passive continental margin as exemplified by the Barents Sea. Mar. Geol. 85 (2–4), 251–272. https://doi.org/10.1016/0025-3227(89)90156-4.

Wang, J., Ikeda, M., 2000. Arctic oscillation and Arctic sea-ice oscillation. Geophys. Res. Lett. 27 (9), 1287–1290. https://doi.org/10.1029/1999GL002389.

Wassmann, P., Andreassen, I., Reigstad, M., Slagstad, D., 1996. Pelagic-benthic coupling in the Nordic seas: the role of episodic events. Mar. Ecol. 17 (1–3), 447–471. https://doi.org/10.1111/j.1439-0485.1996.tb00520.x.

Widdows, J., Brinsley, M.D., Bowley, N., Barrett, C., 1998. A benthic annular flume for in situ measurement of suspension feeding/biodeposition rates and erosion potential of intertidal cohesive sediments. Estuar. Coast. Shelf Sci. 46, 27–38. https://doi.org/10.1006/ecss.1997.0259.